 Q. J. R. Meteorol. Soc. 140: 766–782, April 2014 DOI:10.1002/qj.2200

RMetS
Royal Meteorological Society

Ensemble-based analysis and sensitivity of mesoscale forecasts of a vortex over southwest China

Jun Li[a], Jun Du[b]* Da-Lin Zhang[c], Chunguang Cui[a] and Yishan Liao[a]

[a]*Hubei Key Laboratory for Heavy Rain Monitoring and Warning Research and Wuhan Institute of Heavy Rain of the Chinese Meteorological Administration, Wuhan, China*

[b]*NOAA/NCEP/Environmental Modeling Center, College Park, Maryland, USA*

[c]*Department of Atmospheric and Oceanic Science, University of Maryland, College Park, USA*

*Correspondence to: Jun Du, NOAA/NCEP/Environmental Modeling Center, 5830 University Research Court, College Park, Maryland 20740, USA. E-mail: Jun.Du@noaa.gov

In this study, an ensemble analysis and sensitivity experiment of a mesovortex over southwest China (Southwest Vortex, SWV) are performed with a regional ensemble prediction system in order to demonstrate: (i) the usefulness of an ensemble prediction system for diagnosing the dynamical and thermodynamical characteristics leading to the SWV's eastward movement and growth; and (ii) the potential importance of adopting targeted observations in improving short-range weather forecasts by applying a simple technique. Results show significant variations in forecast performance, ranging from good to poor, among 11 ensemble members. By examining two distinct clusters ('moving' and 'staggering') of the ensemble members it is found that a strong upper-level trough with positive vorticity advection near the vortex centre, its westward vertical tilt and lower-level downstream wet and upstream dry moisture configuration favour the eastward movement and growth of the SWV. Ensemble sensitivity analysis shows that: (i) a simple correlation-based ensemble sensitivity method works well in identifying sensitive areas of mesoscale forecasts of the SWV; (ii) the forecast of the SWV movement and intensity is especially sensitive to initial conditions of horizontal wind and moisture fields; and (iii) unlike the medium-range forecast in which a sensitive region is often traced back to an area far upstream in association with a Rossby-wave packet, sensitive regions in short-range forecasts appear to be directly related to the meteorological system of interest located not far upstream. Based on the results, we suggest that field experiments of targeted observations potentially can be designed using this simple ensemble sensitivity approach to improve short-range weather forecasts associated with SWVs.

Key Words: ensemble prediction system; ensemble sensitivity; Southwest Vortex; ensemble analysis; targeted observation; real-time research

Received 16 November 2012; Revised 18 May 2013; Accepted 20 May 2013; Published online in Wiley Online Library 5 September 2013

1. Introduction

The Southwest Vortex (SWV), a special type of mesoscale convective system (MCS), typically occurs during the growing season in the Sichuan Basin of southwest China (Figure 1). This type of MCS is normally most visible in the lower troposphere, e.g. by a cyclonic circulation at 700 hPa. The SWV often brings extreme weather, especially disastrous heavy rain, to southwest China and the middle and lower Yangtze River valley as it develops and moves eastward out of the Sichuan Basin (Tao, 1980; Lu, 1986; Chen *et al.*, 2003; Chen *et al.*, 2011). Statistically, the severity of heavy precipitation caused by SWVs is ranked second only to that caused by tropical cyclones in China (Wang *et al.*, 1996). Therefore, many observational and modelling studies, including two major Tibetan Plateau scientific field experiments in 1979 and 1998 (Xu and Chen, 2006), have been conducted to examine the formation and development of SWVs.

Unlike mesoscale convective vortices (MCVs) occurring over North America (e.g. Zhang and Fritsch, 1986, 1987, 1988; Bartels and Maddox, 1991; Davis *et al.*, 2004), there are several unique factors that contribute to the formation and subsequent growth of SWVs, as illustrated in Figure 1. First, SWVs are cyclonic circulations topographically forced as the southwestern Asian monsoonal flow climbs and cyclonically turns around the southeast corner of the Tibetan Plateau. Wu and Chen (1985) find that the interaction between the topography and favourable large-scale flows acts as a dynamical mechanism for the formation of SWVs. Second, some SWVs may originate from the eastward propagation of meso-lows over the Tibetan Plateau (Wang, 1987). For example, Chen *et al.*. (2004) and Zhao and Wang (2010) show that SWVs could rapidly deepen vertically as

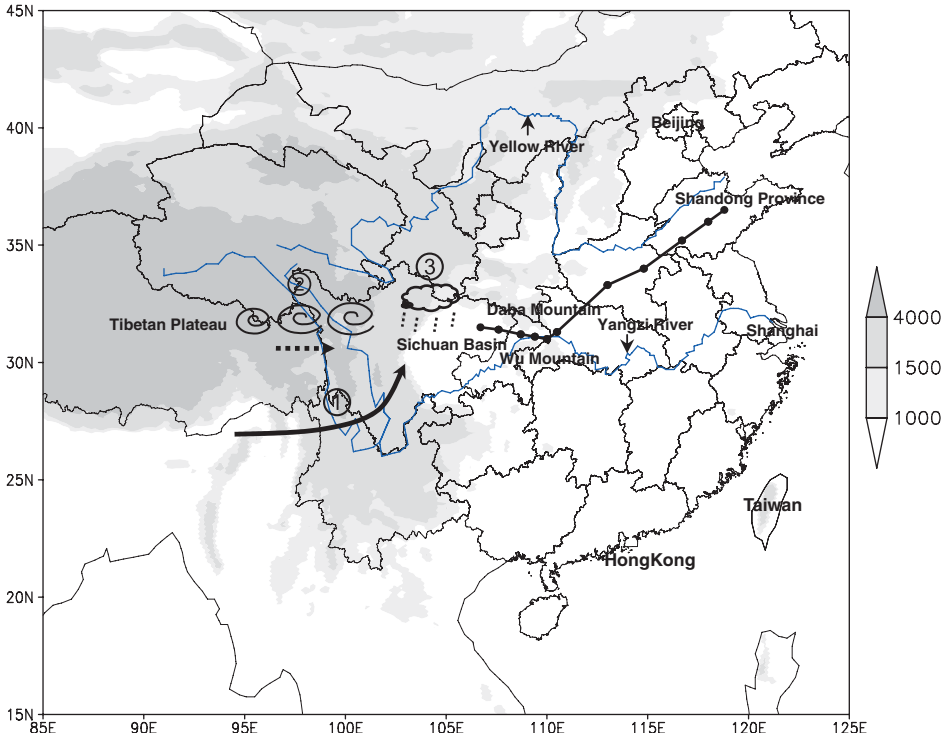

Figure 1. Observed low pressure centre or vortex track at 700 hPa (thick solid line connecting dots) from 1200 UTC on 21 July to 0000 UTC on 24 July 2008, superimposed on the geographical background (elevation is shaded in m) and a sketch of the three known mechanisms for Southwest Vortex formation. The domain covers the model integration area of this study. This figure is available in colour online at wileyonlinelibrary.com/journal/qj

their associated mid-level cyclonic vorticity is advected eastward out of the Plateau and vertically collocated with a low-level weak and shallow baroclinic system. Third, like typical MCVs occurring over North America, latent heat release plays a critical role in the growth of SWVs (Wang and Orlanski, 1987; Kuo *et al.*, 1988; Zhao and Wang, 2010). Wang *et al.*. (1993) and Chang *et al.*. (2000) argue that without the latent heating, dynamical instability and topographical forcing are not strong enough to maintain an intense SWV.

Although there is considerable knowledge on the formation of SWVs, few studies have been conducted to examine the parameters associated with their eastward movement, due partly to the fact that their spatial and temporal scales are too small to be captured by a conventional observational network. In addition, the presence of the Daba and Wu Mountains in the upper Yangtze River valley (Figure 1) tends to 'obscure' the cyclonic circulations of SWVs such that their mesoscale characteristics are not clearly traced. As a result of the difficulty in predicting whether it will move eastward or not, their subsequent growth and the intense precipitation they produce after moving out of the Sichuan Basin is a challenge for operational forecasters in China (Wang and Gao, 2003). Using a mesoscale adjoint model, Wang and Gao (2003) performed a sensitivity case study on the eastward movement of a SWV and found that it is particularly sensitive to the following initial conditions (ICs) over southwest China: westerly winds below 400 hPa, southerly winds below 500 hPa and the temperature field in the 500–900 hPa layer. They also found that adding cyclonic wind perturbations in the lower troposphere favours the formation and eastward movement of the SWV, while moistening the lower troposphere increases its intensity and accelerates its eastward movement.

The objectives of this study, by using a SWV as an example, are to: (i) diagnose the dynamical and thermodynamical characteristics leading to the eastward movement of SWVs by using a regional ensemble prediction system (REPS) based on weather research and forecast (WRF) to demonstrate the use of ensemble forecast data as a tool to understand meteorological processes of a weather system; and (ii) show whether or not such a REPS potentially can be used with adaptive or targeted observations in order to improve short-range weather forecasts of SWVs with a rather simple technique. The first objective will be achieved by analysing the differences between two distinct groups of the ensemble members of a SWV that was formed on 21 July, 2008. Currently, either observational study or numerical experiments are used to understand why a weather system develops or does not develop. In observational study, researchers need to collect observations to include many similar cases of their interest. In numerical simulations, researchers need to design and run special experiments by altering initial conditions or physics schemes to understand why a weather system performs differently. In both of these traditional approaches, preparatory efforts and special design are required. In the first part of this article (excluding the sensitivity experiment), we aim to demonstrate a new approach that can be used to perform a prompt research (i.e. real-time research) that does not involve pre-preparation, but analyses a readily available ensemble of operational data for a particular case to quickly gain insight into why such a weather system develops or does not develop. In addition, one advantage of such a method over an observational study is that the exact same synoptic background is used, whereas similar cases with probable different synoptic backgrounds are used in an observational study. The second objective is to perform an 'ensemble sensitivity' analysis using all REPS members. As we know, targeted observations have been used routinely in experiments in numerical weather prediction (NWP), especially medium range forecasts during cold seasons, such as in the Fronts and Atlantic Storm Track Experiment (FASTEX) (Snyder, 1996; Joly *et al.*, 1997, 1999; Emanuel and Langland, 1998; Bergot, 1999), the North Pacific Experiment (NORPEX-98; Langland *et al.*, 1999) and the Winter Storm Reconnaissance Program at the US National Centers for Environmental Prediction (NCEP) (Szunyogh *et al.*, 2000, 2002; Toth *et al.*, 2000), as well as in hurricane forecast experiments during warm seasons (Burpee *et al.*, 1996; Aberson, 2010). However, little attention has been paid to the short-range NWP of warm-season mesoscale systems over land, which is the focus of this study. In addition to the differences in weather system choice and time range considered, the methods used in these early experiments were rather complex, such as singular vector or ensemble transform techniques. In contrast a much simpler statistical method was tested in this

study. Readers need to bear in mind that this study is not a direct study on targeted observations but rather 'a proof of concept' study through sensitivity experiments, which has an obvious implication for targeted observations for warm-season mesoscale NWP in the short time range.

The next section describes the larger-scale conditions associated with the SWV case, the REPS and data used for this study. Section 3 presents a diagnosis of the SWV track and development. Section 4 shows the results from 'ensemble sensitivity' experiments. A summary is given in the final section, with a discussion.

2. Case overview and model description

The selected SWV was a high-impact event that formed in the eastern Sichuan Basin on 21 July 2008 under the influence of an eastward-moving plateau vortex around the southeast corner of the Tibetan Plateau (Zhao and Wang, 2010). The synoptic conditions at 1200 UTC on 21 July are given in Figure 2(a), showing that the central Sichuan Basin was dominated by a mesoscale trough at 500 hPa, with a closed cyclonic circulation visible at 700 hPa that is the SWV of our focus. The 850 hPa map exhibits strong flows (low-level jets) at both the northwest and

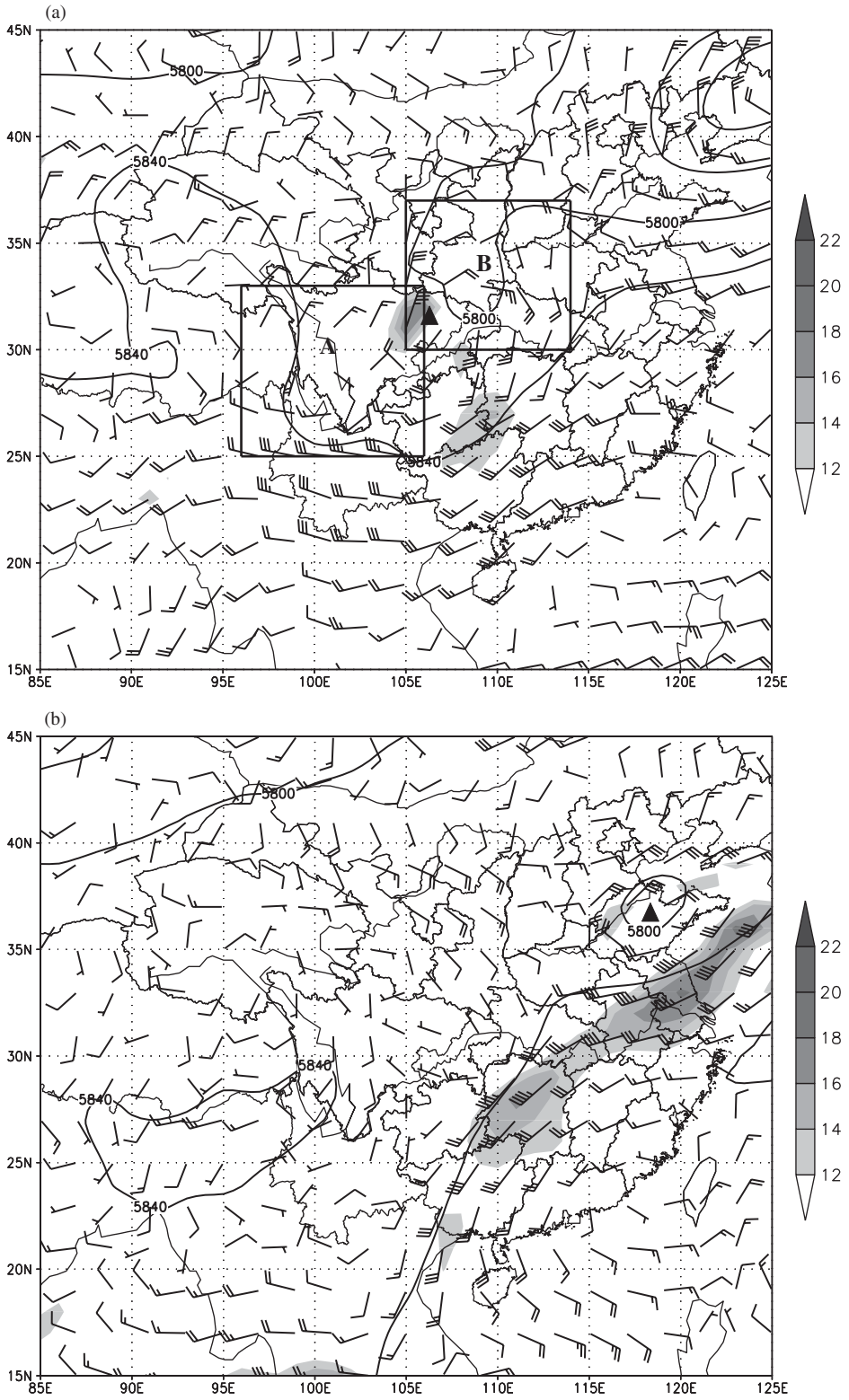

Figure 2. Synoptic conditions of the geopotential heights at 500 hPa (m, contoured) and flow vectors at 700 hPa with the 850 hPa jets shaded (m s^{-1}) at (a) the model initial time (i.e. 1200 UTC on 21 July) and (b) the model ending time (i.e. 0000 UTC on 24 July). Triangle indicates the observed Southwest Vortex centres at 700 hPa. Boxes A and B in (a) are the two selected sensitive regions discussed in section 4.2.

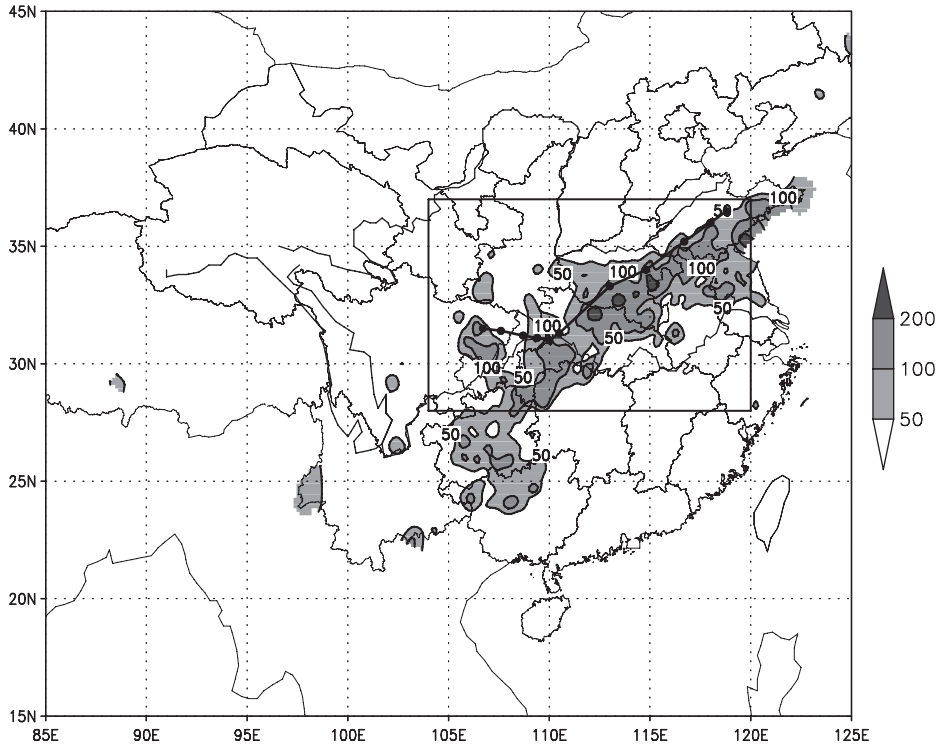

Figure 3. Observed 72 h accumulated precipitation (shaded in mm) from 0000 UTC on 21 July to 0000 UTC on 24 July 2008 along with the observed SWV track (thick solid line connecting dots) from 1200 UTC 21 to 0000 UTC 24 July 2008. The outer domain is for model integration and the inner domain is for the area of interest.

southeast sides of the SWV. The SWV moved eastward over the next 60 h, crossing Daba Mountain, and then northeastward to Shandong Province in the lower Yellow River valley (cf. Figures 1 and 2(b)). With ample moisture supply from southwesterly monsoonal flows, the SWV left behind a large area of heavy rainfall exceeding 100 mm, with a few centres of over 200 mm during the period from 0000 UTC on 21 July to 0000 UTC on 24 July (Figure 3).

The REPS used in this study is a WRF-based mesoscale ensemble prediction system tailored for heavy precipitation forecasts developed at the Wuhan Institute of Heavy Rain (Li *et al.*, 2009). The dynamical core is the WRF model Version 2.1.1 developed by the National Center for Atmospheric Research (NCAR) (Skamarock *et al.*, 2005). The model has 31 vertical levels and a horizontal resolution of 45 km with a (x, y) domain coverage of about 4000 km × 3000 km (85°E–125°E, 15°N–45°N) centred at the point (105°E, 30°N; see Figure 1). It is initialized at 1200 UTC on 21 July 2008 using the real-time operational NCEP global forecast system (GFS) analysis as the control ICs, and integrated for 60 h ending at 0000 UTC on 24 July 2008. To mimic the NCEP's short-range ensemble forecast (SREF) system (Du *et al.*, 2009), ICs are perturbed by the Breeding method (Toth and Kalnay, 1993) using a 12 h forecast cycle with rescaling to create 11 ensemble members (1 control and 10 perturbed; see Li *et al.*. (2009) for a detailed description of perturbing ICs). To increase diversity, forecasts from different members of the NCEP real-time operational T126 (∼110 km) global ensemble prediction system* (Tracton and Kalnay, 1993; Wei *et al.*, 2008) are used as the lateral boundary conditions (LBCs) for different REPS members (where the global control member is used for the REPS control member). In order to realistically simulate large-scale environmental flows, the model integration domain (i.e. the outer domain in Figure 3) is much larger than the area of interest for the purpose of our analysis (the inner domain in Figure 3, roughly 1100 km × 1700 km, 25 × 40 grid points). The NCEP GFS analysis and Chinese Meteorological Administration's rain-gauge precipitation observations are used as the ground-truth in the study.

3. Analysis of the vortex's eastward movement from distinct ensemble clusters

Figure 4 compares the SWV three-hourly track forecasts from the 11 ensemble members to the observed. It is apparent from Figure 4 that seven members (ctl, m1, m3, m5, m7, m8 and m10) are quite successful, whereas the other four members (m2, m4, m6 and m9) completely fail by comparing their forecasted vortex positions with the observed position at 60 h. Most of the successful members are, however, about 6–12 h slower than the observed positions. It is also interesting to note that the vortex track seems to be less predictable during the first 24 h than the later period, due probably to the above-mentioned mountain-blocking effect. For the sake of the subsequent discussion, we denote the six members in the first group (ctl member is excluded because it has no perturbation added in IC) as the 'eastward moving or moving' cluster and the four members in the second group as the 'locally wandering or staggering' cluster.

3.1. *Differences between the moving and staggering clusters*

To gain insight into the factors that are favourable for the development, especially the eastward movement, of the 21 July 2008 SWV, we examine the differences in the IC perturbations and their time evolution between the moving and staggering clusters. For this purpose, the following three types of analyses of the IC perturbations are performed: (i) their vertical profiles at the point (31.5°N, 106.5°E) where the vortex centre (at 700 hPa) of the control member is located at the initial time; (ii) their zonal (102–112°E) vertical cross-sections through the vortex centre (along the latitude of 31.5°N); and (iii) their horizontal structures. To have a robust result, all the differences displayed in the following Figures (5)–(9) are composite ones, which are averaged over all the members in either the moving group or the staggering group. Generally speaking, the resulting differences of

*As the NCEP global ensemble is the only system available to us free of charge in real time and high quality, it is used in our operational regional ensemble prediction system to provide the LBCs.

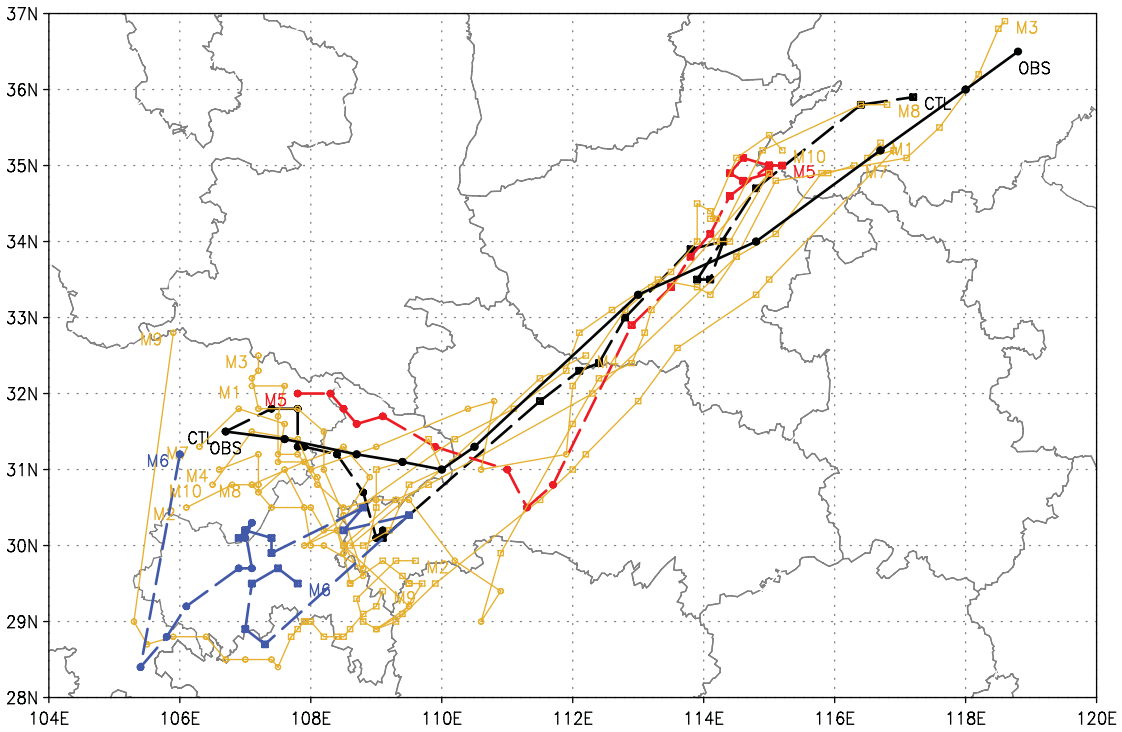

Figure 4. Six-hourly observed Southwest Vortex (SWV) track (black solid) and three-hourly predicted SWV tracks at 700 hPa from 11 ensemble members from 1200 UTC on 21 July to 0000 UTC on 24 July 2008: the control member (black dashed), the representative 'moving' member/M5 (red dashed), the representative 'staggering' member/M6 (blue dashed), and the other perturbed members (golden solid).

the two groups are similar in spatial distribution but opposite in phase. The details are analysed below.

Figure 5(a) compares the vertical profiles of the initial height perturbations at the SWV centre between the moving and staggering clusters. We see large negative perturbations below 500 hPa favouring the lower-tropospheric cyclonic generation and convergence, large positive perturbations above 300 hPa enhancing the upper-level anticyclonic generation and divergence, and small but generally negative perturbations in between for the moving cluster, whereas the opposite is true for the staggering cluster. A zonal vertical cross-section of the moving cluster through the vortex centre, given in Figure 5(b), shows the presence of negative/cyclonic (positive/anticyclonic) height perturbations below (above) 350 hPa on the east side or downstream of the vortex, while the initial height perturbations on the west side or upstream of the vortex are smaller but opposite in sign, which is consistent with Figure 5(a). To help examine the vertical structures of the initial vortex, Figure 5(c) displays the zonal vertical cross-section along 31.5°N for the height deviation (h'), which is defined as a height departure from its zonal mean value (which is averaged over the 102°E–112°E range) at individual pressure levels for the moving cluster (dashed), staggering cluster (dotted) and control (solid) member. All of them exhibit a negative h' centre (viewed as the vortex centre), as enclosed by the contour of −10 m, where it can be seen that the vertical axis connecting the main lower-level and upper-level low centres has a greater (smaller) westward tilt of the moving (staggering) cluster's vortex with a stronger (weaker) h' value at the lower-level centre than that of the control member. Similarly, Figure 5(d) shows generally negative (positive) sea-level pressure (SLP) perturbations in the eastern and northern (southwestern) quadrants of the moving cluster's vortex, whereas the sign is generally opposite for the staggering cluster's vortex (not shown).

These height and SLP perturbations are hydrostatically consistent with the vertical thermal perturbations. That is, the moving cluster's vortex is characterized with warmer (colder) temperature perturbations in the 700–500 hPa and 250–150 hPa (400–300 hPa and 900–800 hPa) layers; the opposite is true for the staggering cluster's vortex (Figure 6(a)). Although similar vertical alternations of temperature perturbation can be seen in Figure 6(b), but in a larger picture, Figure 6(b) displays generally warmer (colder) columns from the centre to the east (west) of the moving cluster's vortex below 200 hPa, relative to those in the control vortex. Such cold–warm temperature contrast will enhance the baroclinic instability development of the vortex through cold and warm air advections. All these – the more negative perturbations in height and SLP from the vortex centre to its downstream area (resulting in favourable vorticity and divergence distribution in space), the larger westward vertical tilt structure and the increased baroclinic instability from the enhanced temperature contrast – are likely to create a more favourable vortex environment for the moving members to grow more and move eastward at a faster rate than that of the staggering members.

As latent heat release plays an important role in the growth of SWVs (Wang and Orlanski, 1987; Kuo *et al.*, 1988; Wang *et al.*, 1993; Chang *et al.*, 2000; Zhao and Wang, 2010), Figure 7 compares the vertical structures of the initial specific humidity perturbations between the moving and staggering clusters. A general moisture reduction (increase) is seen near the vortex centre with large perturbations below 800 hPa and in the 600–350 hPa layer, and small perturbations in between (i.e. 800–600 hPa) for the moving (staggering) members (Figure 7(a)). This middle- to upper-level moisture reduction (increase) is more obvious in the relative humidity field (not shown), due to the colder (warmer) temperature perturbation between 500 and 250 hPa (cf. Figures 7(a) and 6(a)). Of interest is that the zonal vertical cross-section of the moving cluster (Figure 7(b)) reveals a generally wetter environment on its east side (downstream), with the peak moisture perturbation occurring near 600 hPa, as compared with that in the control member. This moisture configuration is consistent with the moisture transport in the southwesterly monsoonal flows in the forward semicircle of the vortex circulation. However, generally dryer conditions are observed at the vortex centre as well as on its west side (upstream) for the moving members. Such an asymmetric moisture distribution tends to favour more latent heat release in the warm and moist southwesterly flow branch, and to force the vortex to move eastward as a result of the vortex stretching

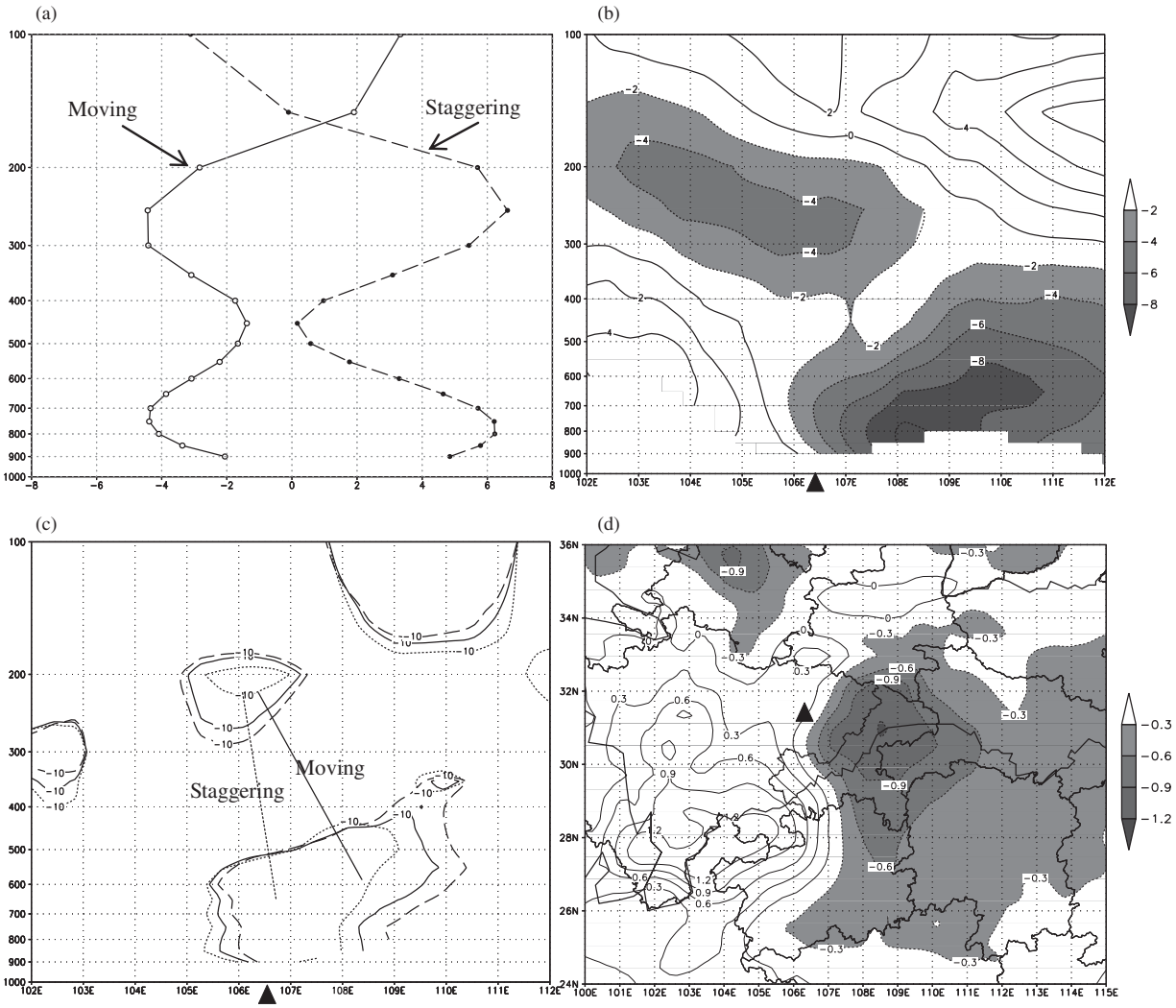

Figure 5. Composite initial-perturbation differences between the 'moving' and 'staggering' clusters: (a) the vertical profiles of initial geopotential height perturbations at the Southwest Vortex (SWV) centre, 31.5°N,106.5°E (solid for the 'moving' and dashed for the 'staggering' clusters); (b) the vertical cross-section of the 'moving' cluster's initial geopotential height perturbations along 31.5°N from 102°E to 112°E; (c) the vertical cross-section along 31.5°N of the departures of a member's geopotential height from its zonal mean value averaged over 102°E–112°E (solid for the control member, dashed for the 'moving' cluster, and dotted for the 'staggering' cluster), where negative centres (enclosed by −10 m contour) can be viewed as the SWV centre area, and the estimated vertical axis connecting the main low-level and upper-level low centres of the 'moving' and 'staggering' clusters are also illustrated; and (d) the spatial distribution of initial SLP perturbations of the 'moving' cluster. Units: geopotential height in metres and SLP in hPa. Triangle indicates the location of the SWV centre of the control member.

associated with diabatic heating (Zhang and Fritsch, 1987). More evidence related to the impact of latent heat release can be seen from the subsequent precipitation development, which will be discussed in section 3.2.

Figure 8 compares the vertical structures of perturbations of the initial wind components u and v between the two groups. At the upper level (above 400 hPa), a stronger (weaker) trough presents aloft for the moving (staggering) cluster. Thus, the enhanced northwesterly flow in the west (upstream) intensifies the vortex and the enhanced southwesterly flow over the vortex centre advects positive vorticity downstream, to make the vortex propagate northeastward for the moving cluster. At the lower level (below 600 hPa) the u perturbations are generally small (Figure 8(c)), but northerly flow is enhanced in the upstream of the vortex centre region and southerly flow is enhanced in the downstream region (east of 108°E) (Figure 8(d)) for the moving cluster. The enhanced southerly flow pushes the lower-level convergence zone northeastward (not shown) as well as transporting moisture, and fuels latent heat release through precipitation downstream, while the enhanced northerly flow infuses dry air and suppresses precipitation upstream and near the vortex centre region (Figure 9(a)). The combined effect of the above should lead to downstream development of the vortex and, therefore, to the SWV vortex moving northeastward, with the opposite being true for the staggering cluster.

To evaluate the validity of the above conjectures, we have examined the time evolution of the IC perturbations in the moving and staggering clusters during their first 12 h model integrations. We find that the relative differences between these two distinct groups after the 12 h integrations are qualitatively similar to those at the initial time, so the associated results are not shown but summarized as follows, mainly from our 700 hPa analysis.

(a) Negative (positive) height perturbations are distributed in the eastern semicircle of the moving (staggering) cluster's vortex, indicating the generation of a more (less) intense vortex and more (less) favourable eastward movement.
(b) Warmer (cooler) columns are distributed in the core region of the moving (staggering) cluster's vortex, suggesting more (less) favourable development.
(c) A drier (wetter) environment is found in the western (eastern) semicircle of the moving cluster's vortex, whereas the opposite is true for the staggering cluster. Similarly, more precipitation falls in the eastern semicircle of the moving cluster's vortex (Figure 9(a)), whereas more precipitation falls in the western semicircle of the staggering cluster's vortex (Figure 9(b)). It is, therefore, reasonable to infer (also supported by previous studies) that more latent heat release on the eastern portion facilitates the downstream generation of cyclonic vorticity, favouring the

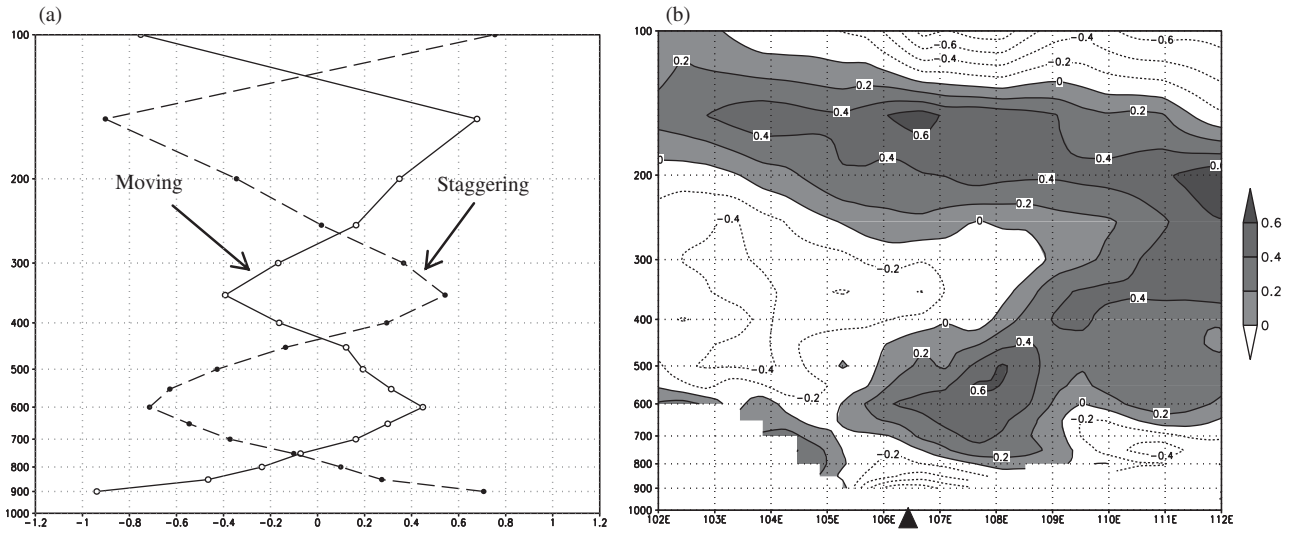

Figure 6. As in Figure 5(a) and (b), but for temperature perturbations (°C).

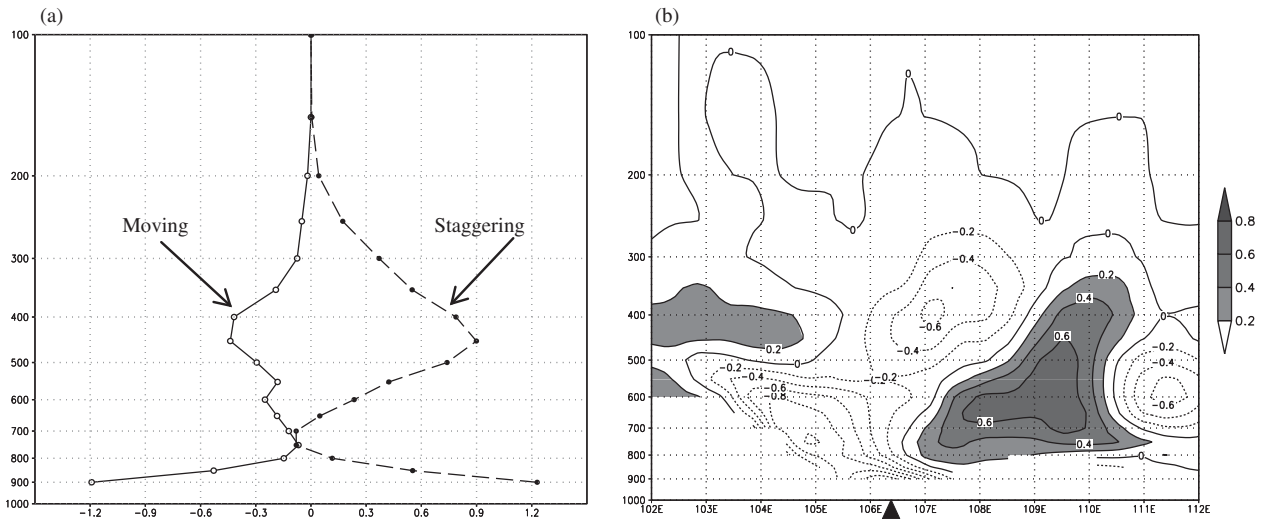

Figure 7. As in Figure 5(a) and (b), but for specific humidity perturbations (g kg^{-1}).

eastward movement of the vortex, as will be further seen in the next section.

(d) A stronger (weaker) upper-level trough and enhanced (reduced) lower-level northerly flow in the upstream region and vortex centre and enhanced (reduced) southerly flow in the downstream region are seen for the moving (staggering) clusters. As a result, the moving SWVs become better developed and move eastward out of the Sichuan Basin after 24 h, as observed, whereas the staggering SWVs wander and later decay locally (Figure 4).

Based on the above analyses, we may state that favourable conditions in the ICs for the growth and eastward movement of the SWV are: (i) lower height and SLP in the downstream semicircle with greater westward vertical tilt of the vortex; (ii) stronger cold/warm air contrast (baroclinicity) within the closed circulation, with more (less) moisture distributed downstream (upstream), and stronger trough aloft; (iii) stronger dry air intrusion from the north in the upstream and vortex centre regions; and (iv) stronger moisture transportation from the south in the downstream region at lower levels.

3.2. *Sensitivity to IC perturbations: full-domain experiments*

After observing all these IC perturbation differences in various variables between the moving and staggering clusters, we were motivated to examine which IC variable(s) might play a more important role in determining the track and intensity forecasts of the SWV. As geopotential height is not a directly perturbed field, only moisture, wind, temperature and SLP were tested in the following four numerical experiments, referred to as FD_ALL_humi/wind/temp/mslp (Table 1(a)), to examine the model's sensitivity to each of them. A pair of representative members, m5 and m6, were used for these experiments, where m5 represents an eastward-moving member and m6 a locally wandering (staggering) member (see the red and blue tracks in Figure 4). To do so, a selected IC field in the staggering m6 member is replaced by its corresponding IC field from the moving m5 member at all levels (ALL) over the model full domain (FD), while holding all the other model parameters identical to those in the staggering m6 member. Specifically, in Experiment FD_ALL_humi the initial three-dimensional specific humidity field in the staggering m6 member is replaced by that of the moving m5 member, while keeping all the other initial fields unchanged. The same procedure is applied to the initial horizontal winds for Experiment FD_ALL_wind, the initial temperature field for Experiment FD_ALL_temp and the initial mean SLP field for Experiment FD_ALL_mslp. Table 1(a) describes these full-domain sensitivity experiments. By changing one IC field and keeping others the same, there may be concern that it could cause imbalance to ICs. As anything altered in ICs here is merely a small perturbation (difference between ensemble members), the magnitude of which was controlled to be within the uncertainty level of this particular field in the Breeding procedure (Toth and Kalnay, 1993; Li *et al.*, 2009), replacing an IC field should not cause ICs to be apparently imbalanced in forecasts. To confirm

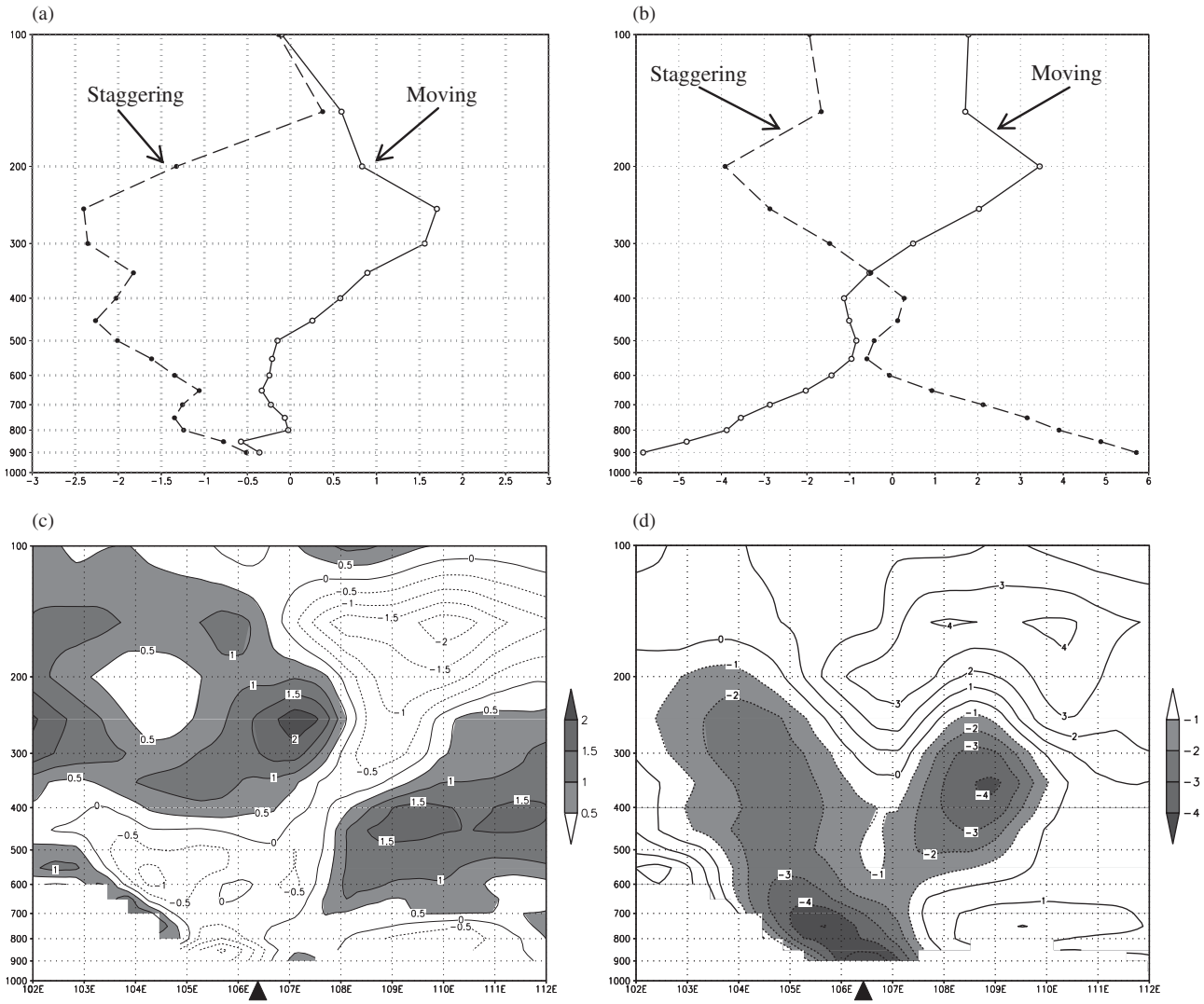

Figure 8. As in Figure 5(a) and (b), but for u perturbations ((a) and (c)) and v perturbations ((b) and (d)). Unit: m s^{-1}.

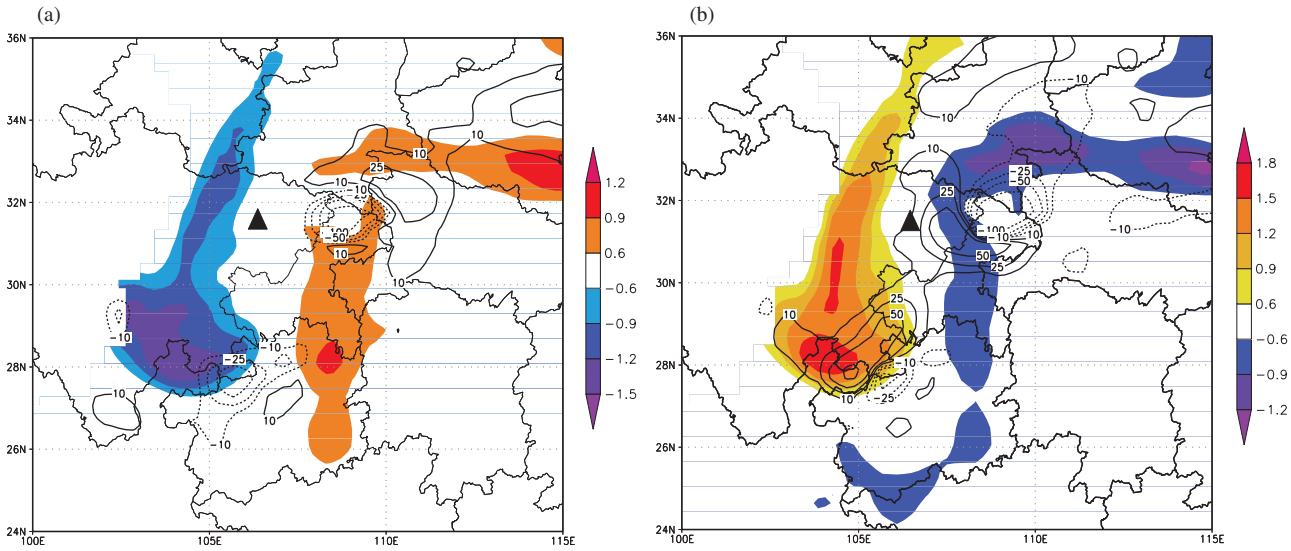

Figure 9. Relationship between the initial specific humidity perturbations (g kg^{-1}) at 700 hPa (colour shaded) and the subsequent 12 h precipitation (mm) forecast departures from the control member (contoured) for the (a) 'moving' cluster and (b) 'staggering' cluster. The triangle denotes the initial vortex position of the control member.

this, we have examined the time evolution of all perturbation fields from all the numerical experiments performed in this study (including the four FD_ALL experiments in this section and the other 16 experiments in section 4.3). Our result shows that the differences in all 20 experiments evolve smoothly with time, similar to the behaviour of the differences between the two original unaltered ensemble members (not shown). Therefore, no obvious imbalance is introduced in the ICs in our experiments, although slight imbalance is expected theoretically.

The predicted tracks from the four experiments are given in Figure 10, showing that after replacing either the moisture (FD_ALL_humi) or the horizontal wind (FD_ALL_wind) field, the

Table 1. The 20 numerical sensitivity experiments performed in this study.

Name	Description	Purpose
(a) The full-domain (FD) sensitivity experiments		
FD_ALL_humi	Replacing staggering member's initial *Q* at all levels with that of moving member's over full model domain	Sensitivity to initial moisture
FD_ALL_wind	Replacing staggering member's initial *u*, *v* at all levels with those of moving member's over full model domain	Sensitivity to initial wind
FD_ALL_temp	Replacing staggering member's initial *T* at all levels with that of moving member's over full model domain	Sensitivity to initial temperature
FD_ALL_mslp	Replacing staggering member's initial SLP with that of moving member's over full model domain	Sensitivity to initial sea-level pressure
(b) First group of the local-area sensitivity experiments		
A/B_ALL_humi	Replacing staggering member's initial *Q* at all levels with that of moving member's within region A/B	Sensitivity to initial moisture within A/B
A/B_ALL_wind	Replacing staggering member's initial *u*, *v* at all levels with those of moving member's within region A/B	Sensitivity to initial wind within A/B
A/B_ALL_temp	Replacing staggering member's initial *T* at all levels with that of moving member's within region A/B	Sensitivity to initial temperature within A/B
A/B_ALL_mslp	Replacing staggering member's initial SLP with that of moving member's within region A/B	Sensitivity to initial sea-level pressure within A/B
(c) Second group of the local-area sensitivity experiments		
A/B_PART_llq	Replacing staggering member's initial *Q* at lower levels (below 500 hPa) with that of moving member's within region A/B	Sensitivity to lower-level moisture within A/B
A/B_PART_ulq	Replacing staggering member's initial *Q* at upper levels (above 500 hPa) with that of moving member's within region A/B	Sensitivity to upper-level moisture within A/B
A/B_PART_llw	Replacing staggering member's initial *u*, *v* at lower levels (below 500 hPa) with those of moving member's within region A/B	Sensitivity to lower-level wind within A/B
A/B_PART_ulw	Replacing staggering member's initial *u*, *v* at upper levels (above 500 hPa) with those of moving member's within region A/B	Sensitivity to upper-level wind within A/B

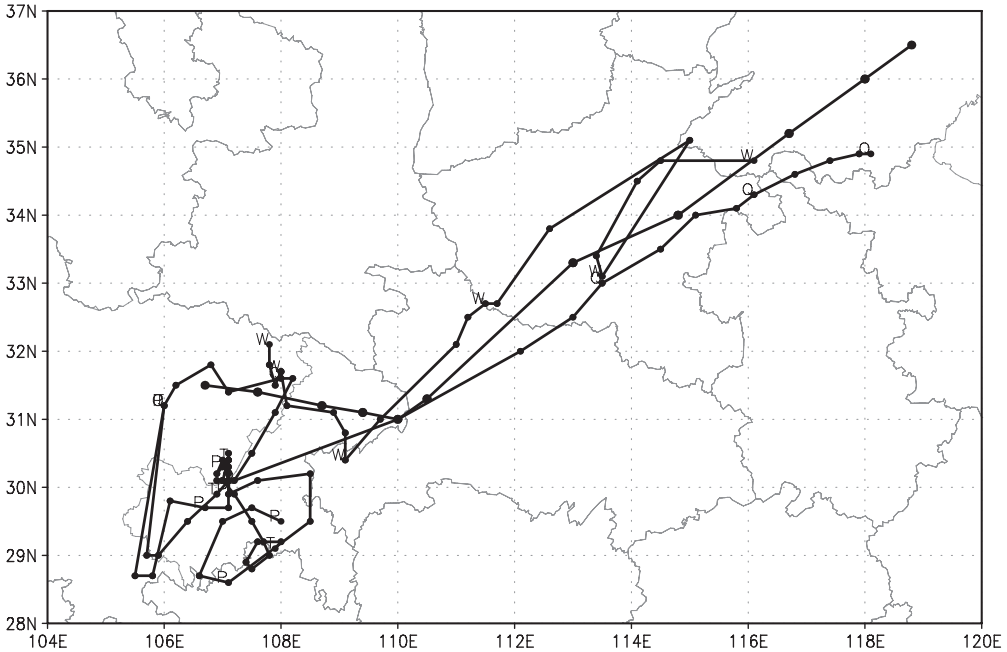

Figure 10. The predicted vortex tracks from the full-domain sensitivity experiments FD_ALL_humi/wind/temp/mslp together with the observed track (thick solid line with filled circles), where FD_ALL_humi is labelled 'Q', FD_ALL_wind 'W', FD_ALL_temp 'T' and FD_ALL_mslp 'P'.

originally quasi-stationary SWV in the staggering m6 member can now successfully move eastward out of the Sichuan Basin, as in the moving m5 member. On the other hand, by replacing either the temperature (FD_ALL_temp) or the mean SLP (FD_ALL_mslp) field in the staggering m6 member, little is improved in the associated forecasts. Thus, we may state that it is the initial wind and moisture fields that account for most of the growth and eastward movement of the SWV. By further comparing Experiments FD_ALL_humi and FD_ALL_wind, we see that the SWV is more stationary (moves much faster) in the 'replaced moisture' experiment than in the 'replaced wind' experiment during (after) the first 24 h integrations. This implies that in the early stage (i.e. 0–24 h) the horizontal wind perturbations play a more important role in the SWV's eastward movement, mainly by strengthening the upper-level trough aloft and enhancing the lower-level southerly flow in the downstream region, whereas the moisture perturbation field dominates the later (i.e. after 24 h) growth stage of the SWV. The delayed moisture impact should be understandable because it would require a certain period of time for the precipitation to spin up, given the 'cold start' of the ensemble forecasts. This delay of the moisture impact also implicitly reflects the importance of latent heat release to the SWV development.

Although an in-depth analysis to the physical and dynamical processes is not the focus of this work, we will attempt to interpret what is going on based on our understanding. Now, the question might arise as to why the SWV's eastward movement is more sensitive to the initial moisture and wind perturbations

instead of the temperature and SLP perturbations. This has something to do with the generation of more precipitation in the eastern portion of the SWV. Specifically, a greater increase in the moisture content of the southerly flow facilitates the generation of precipitation in the eastern portion of the moving member's vortex (Figure 9(a)), which in turn helps increase the local production of cyclonic vorticity ahead of the vortex centre (not shown) through the vortex stretching, thereby forcing the vortex to move eastward as discussed earlier. By comparing the initial moisture perturbations in the 700 hPa level (colours in Figure 9) with the 12-h forecast precipitation perturbations (contours in Figure 9), the forecast asymmetric rainfall is clearly related to the asymmetric moisture perturbation at the initial time. As compared with the control member, the moving member's vortex is initially more (less) moist in the northeast (southwest, south and centre) region of the vortex (Figure 9(a)), whereas the opposite is true for the staggering member's vortex (Figure 9(b)). Correspondingly more rainfall occurs on the east side, especially the northeastern quadrant of the moving member's vortex after the 12 h integration (Figure 9(a)), but more rainfall occurs on the west side, especially the southwestern quadrant of the staggering member's vortex (Figure 9(b)). Thus, it is reasonable to argue that the enhanced diabatic heating in the eastern portion of the SWV drives its eastward movement. On the other hand, according to the geostrophic adjustment theory (Blumen, 1972), a mass field tends to adjust to the wind field for such a meso-α-scale system. Therefore, due to their slightly imbalanced nature, most of the mass (i.e. temperature) perturbations at the vortex scale tend to be propagated away by inertial gravity waves. The remaining temperature perturbations may be adjusted to the horizontal wind field. Similarly, any added perturbations in the surface pressure through SLP tend to appear as external gravity waves, which would propagate away much faster than the internal gravity waves. Thus, we see that replacing the temperature and SLP fields has little impact on the improvement of the growth and eastward movement of the SWVs in the FD_ALL_temp and FD_ALL_mslp runs.

The above results demonstrate that ensemble forecast can provide a readily available basis for understanding the dynamical and thermodynamical characteristics of mesoscale weather systems, as well as quantifying forecast uncertainties (Du, 2007). For example, by analysing the common differences between the two distinct clusters – moving and staggering members – in the present case, we could gain insight into certain flow structures that are favourable for the growth and eastward movement of the 21 July 2008 SWV.

4. Ensemble sensitivity experiments

4.1. Background on ensemble sensitivity

The adaptive or targeted observation strategy is a useful approach, where the location, time and/or observing variables are pre-chosen, to optimize NWP quality (Emanuel and Langland, 1998; Palmer *et al.*, 1998; Bergot *et al.*, 1999; Buizza and Montani, 1999; Morss *et al.*, 2001; Bishop and Toth, 1999; Langland, 2005). Anderson (2001) suggests ensemble-based adaptive 'observations' for data assimilation. A similar method is used by Hamill and Snyder(2002) and Hamill *et al.*. (2002) to study the sensitivity of the analysis to observations. Torn and Hakim (2008) propose an ensemble sensitivity (ES) method as shown in Eq. (1). Torn and Hakim (2008) show that the ES method is a very convenient and effective approach to determine the climatological sensitivity for a selected forecast object without extra model integration. After comparing the adjoint-model-based and ES-based approaches, Ancell and Hakim (2007) find that the ES method can accurately estimate the impact of ICs on a selected forecast object and could be applied to targeted observations. As compared with an adjoint-model-based method, the ES method has the following advantages: (i) it is much cheaper computationally because analysis error information has already been included in the ensemble forecasts and there is no need to separately run a linear adjoint model; (ii) unlike an adjoint model, which is based on some assumptions such as linearity and dry physics, the ES method is a model based on nonlinear full-physics and, therefore, is probably more realistic; and (iii) unlike an adjoint-model-based approach, which is normally targeted or optimized for a particular range (e.g. medium or short range) of forecasts, it is more general for any forecast period. The *ES* of a forecast object J at the forecast time (t) to a model state variable x at initial time t_0 is defined (Ancell and Hakim, 2007; Hakim and Torn, 2008) by

$$ES_i = \frac{\mathrm{cov}(J, x_i)}{\sqrt{\mathrm{var}(x_i)}} = \mathrm{cor}(J, x_i) \times \sqrt{\mathrm{var}(J_i)} \qquad (1)$$

where i represents any location or a grid point within a domain. For an N-member ensemble, $\mathrm{cov}(J, x)$ is a covariance between J and x, $\mathrm{var}(x)$ is a variance of x, $\mathrm{cor}(J, x)$ is a correlation coefficient between $J$and x, and $\mathrm{var}(J)$ is a variance of J, calculated over N ensemble members. Since $\sqrt{\mathrm{var}(J)}$is a form of the ensemble spread of the forecast object J, which is always a constant for a given ensemble of forecasts, we can further simplify the original ES of Eq. (1) into a mere correlation coefficient in this study, i.e.

$$ES_i = \mathrm{cor}(J, x_i). \qquad (2)$$

Since Eq. (2) is simpler and meteorologically easier to explain, we will use only the 'correlation' in Eq. (2) as our ES measure hereafter. For the present ensemble sensitivity study, the 60 h forecast positions (denoted by longitude) and intensities (denoted by the minimum central height value at 700 hPa) of the SWV from the above-mentioned 11 ensemble members are chosen as the forecast objects J (Table 2) in order to examine how sensitive the SWV position and intensity forecasts are to their ICs (x). The initial geopotential heights at 200, 500, 700 and 850 hPa levels as well as SLP are selected as x, respectively.

4.2. Identification of sensitive regions

Figure 11 shows the ESs of the 60 h forecast SWV positions from the 11 members (Table 2) to the corresponding initial height fields at 200, 500 and 700 hPa and to the initial SLP field. Figure 11(a) shows two major sensitive or high-correlation regions at 200 hPa, i.e. a negative minimum is located near the SWV and a positive maximum on the northeast side of the SWV. Similar 'dipole' structures but with opposite correlation signs are seen in the layers below 500 hPa (Figure 11(b) – (d); i.e. a positive maximum (negative minimum) is located roughly on the west (east) side of the SWV. In addition, these extreme centres are also vertically tilted with height, consistent with the westward tilt of the vortex shown in Figure 5(c), shifting the centres southward toward the lower layers. The two sensitive regions are particularly obvious at 500 hPa (Figure 11(b)). Similar conclusions can be drawn from the correlation between the 60 h forecast SWV intensities (Table 2) and the initial heights at various levels and the initial SLP field (see Figure 12). Of interest is that the ESs derived, respectively, from the forecast SWV positions (Figure 11) and the forecast SWV intensities (Figure 12) are very similar to each other in spatial distribution but with opposite signs in the correlation values. The resulting opposite correlation sign implies that stronger SWVs (i.e. lower heights) tend to move eastward further (resulting in a larger longitude value in the Eastern Hemisphere) probably because they are more organized and, therefore, easier to overcome the mountain blocking. As the ESs are similar, we will focus only on the relationship between the SWV position and ICs hereafter. For the sake of our subsequent discussion, we designate two regions as region A and region B in the upstream southwestern and downstream northeastern quadrants of the SWV, respectively, as denoted by boxes A and B in Figures 11(b) and 12(b) as well as Figure 2(a).

Table 2. Sixty-hour (1200 UTC on 21 July to 0000 UTC on 24 July 2008) forecasts of the central Southwest Vortex position (°E) and intensity (m) at 700 hPa for the 11 ensemble members.

Member	CTL	M1	M2	M3	M4	M5	M6	M7	M8	M9	M10
Position	117.2	116.7	109.6	118.6	112.2	115.2	107.8	116.3	116.8	109.1	115.2
Intensity	3052.6	3038.36	3077.5	3017.47	3052.08	3016.28	3072.07	3019.65	3035.17	3045.91	3009.99

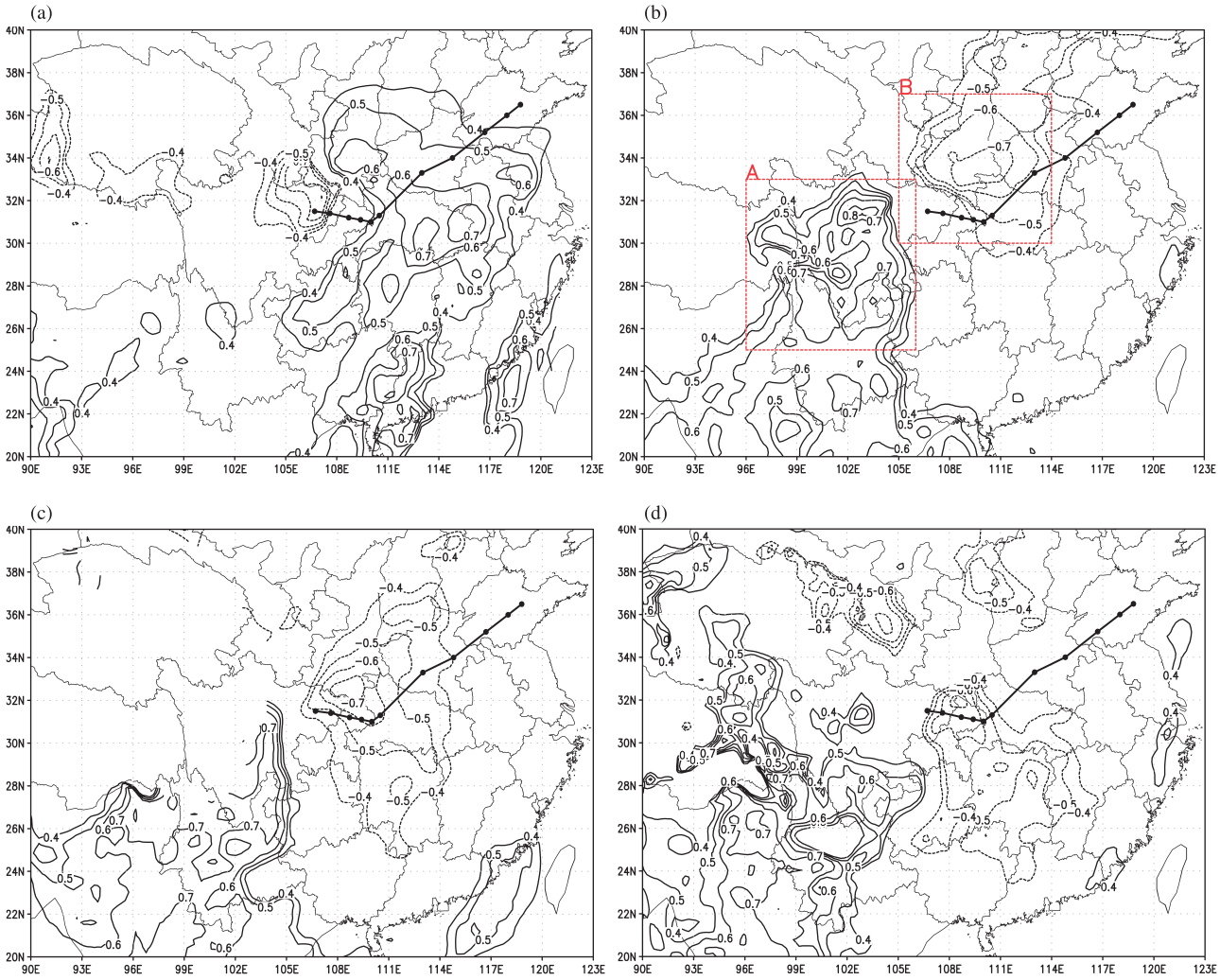

Figure 11. Ensemble sensitivity (Eq. (2)) of the predicted Southwest Vortex positions at 60 h to the initial geopotential heights at (a) 200 hPa, (b) 500 hPa and (c) 700 hPa, and (d) the initial SLP. Boxes A and B in (b) are the two sensitive regions selected. This figure is available in colour online at wileyonlinelibrary.com/journal/qj

The question arises as to whether these two regions are meteorologically meaningful. It is evident from Figure 2(a) that the two regions are located in the northwesterly dry (A) and southwesterly moist (B) flows behind (upstream) and ahead (downstream) of the 500 hPa trough axis, respectively. Based on the results presented in the preceding section most diabatic heating and drying, which determines the growth of the SWV, occurs in the southwesterly and northwesterly flows, respectively. Slight changes in the moisture and wind fields in regions A and B could produce a pronounced impact on the intensity and eastward movement of the SWV. At the same time, the correlation signs of the two sensitive regions revealed by both Figures 11 and 12 are consistent with the analysis results of the moving and staggering clusters discussed in section 3: i.e. a negative height perturbation in the lower layers in the downstream region of the SWV produces a deeper (resulting in a positive correlation with intensity forecasts) and faster eastward-moving (resulting in a negative correlation with position forecasts) vortex. Given the apparent underlying physical connections, these two maximum sensitivity regions at 500 hPa are selected for the further experiments to be discussed in the next subsection. The representative ensemble members m5 and m6 were again used for the following experiments.

4.3. *Sensitivity to IC perturbations: local-area experiments*

Following the same methodology as in the full-domain sensitivity experiments FD_ALL_humi/wind/temp/mslp, as shown in section 3.2, two groups of local-area sensitivity experiments (Tables 1(b) and 1(c)) are carried out by focusing on the impact of the two small selected sensitive regions, rather than the large full-model domain, in order to examine how sensitive the forecast SWV position is to the ICs in either region A or region B. In the first group, a chosen initial field at all the vertical levels (ALL) is modified within a selected box A or B, and in the second group a chosen initial field at only a portion of the vertical levels (PART) is altered within a selected box A or B. Nothing is modified outside of a selected box. As explained in subsection 3.2, no obvious imbalance is introduced in the ICs in these experiments after examining the time evolution of altered IC perturbations (not shown).

Four sensitivity experiments are performed for the upstream sensitive region A by replacing the initial specific humidity (A_ALL_humi), horizontal winds (A_ALL_wind), temperature (A_ALL_temp) and mean SLP (A_ALL_mslp) field in the staggering m6 member, with the corresponding values from

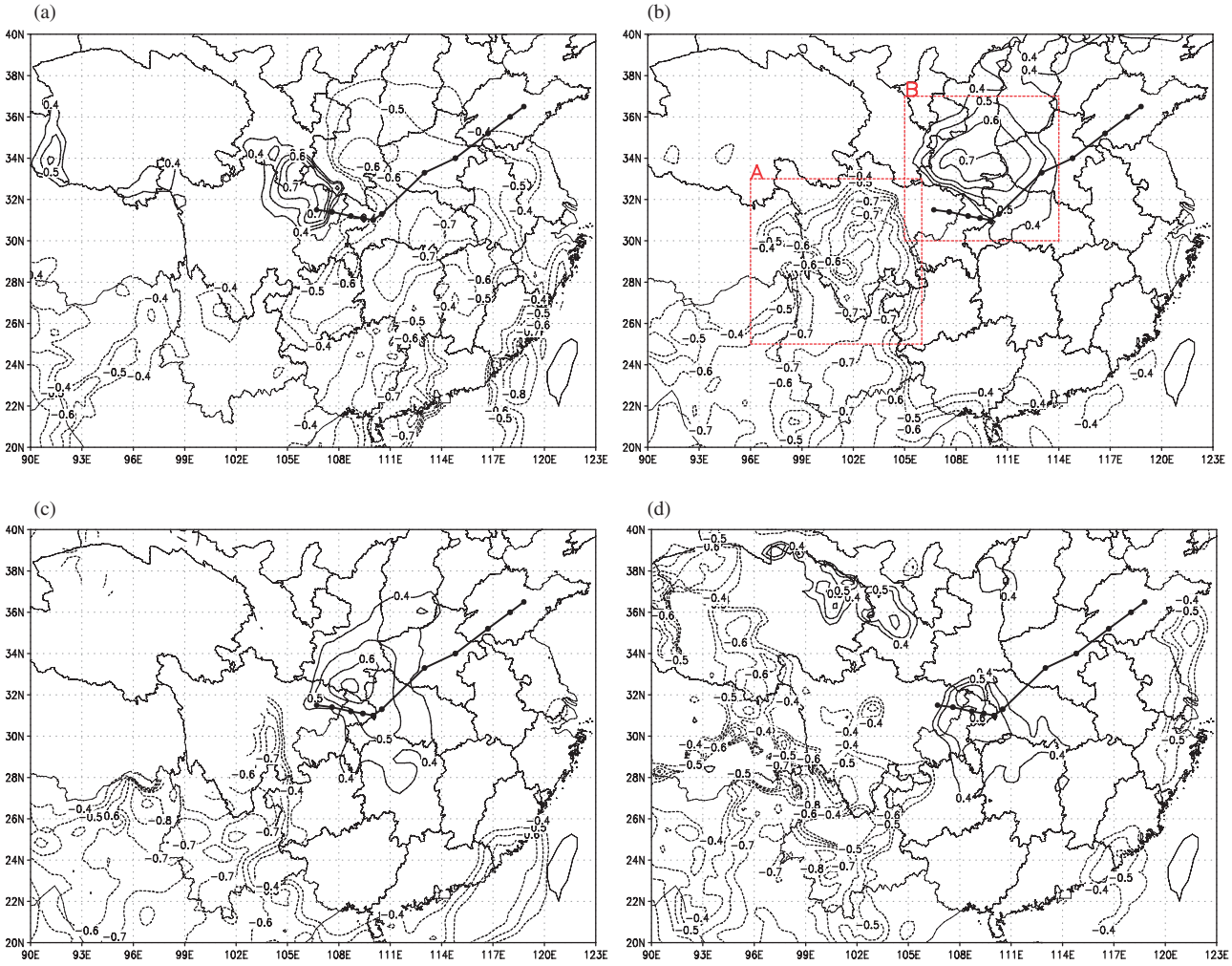

Figure 12. Same as Figure 11 but for the predicted Southwest Vortex intensities at 60 h. This figure is available in colour online at wileyonlinelibrary.com/journal/qj

the moving m5 member (Table 1(b)). The predicted tracks from the four experiments are summarized in Figure 13(a), showing that they are qualitatively similar to the corresponding ones in Experiments FD_ALL_humi/wind/temp/mslp. Namely, replacing either the initial moisture perturbations (A_ALL_humi) or the initial horizontal wind perturbations (A_ALL_wind) allows the original quasi-stationary SWV in the staggering m6 member to successfully move out of the Sichuan Basin, although its movement is slightly slower than that in FD_ALL_humi/wind in the early stage. (This can also be confirmed in the time evolution of IC differences, i.e. the time evolution of the differences is much slower during the first 12 hours when replacing IC within only a local area than that in the full domain – not shown.) Again, the added horizontal wind perturbations play a more important role in the first 24 h of integrations and the added moisture perturbations become more critical with time after the 24 h of integrations in the eastward movement of the SWV, as seen before. In the experiments A_ALL_temp and A_ALL_mslp, replacing either the initial temperature or the initial SLP produces little difference from the original staggering m6 member's vortex forecast.

The above four experiments are then repeated for the downstream sensitive region B, denoted as B_ALL_humi/wind/temp/mslp (Table 1(b)). The associated results are given in Figure 13(b), which is also qualitatively similar to those in Experiments FD_ALL_humi/wind/temp/mslp. That is, the SWV can move out of the Sichuan Basin if either the initial moisture (B_ALL_humi) or the initial horizontal wind (B_ALL_wind) field in region B of the staggering m6 member is replaced by the corresponding field in the moving m5 member, whereas little is changed in the vortex track forecasts when either the initial temperature (B_ALL_temp) or mean SLP (B_ALL_mslp) field is replaced. On the other hand, by carefully comparing Figures 13(a) and 13(b), we see two slight differences between the upstream A and downstream B regions. One is that the SWV position appears to be more sensitive, as indicated by the faster movement or farther eastward distance, to changes in the initial moisture and wind fields in the downstream region B than those in the upstream region A. The other difference is that, as for the SWV eastward movement, the initial wind perturbations play a more important role than the initial moisture perturbations in the downstream region B during both the early (i.e. 0–24 h) and later (i.e. after 24 h) stages, while the initial moisture perturbations play a more important role than the initial wind perturbations in the upstream region A after the 24 h integrations, similar to what happened in the experiments FD_ALL_humi/wind.

Since the SWV position is particularly sensitive to the initial moisture and horizontal wind perturbations in both regions A and B, we were motivated to investigate at which vertical levels the two fields play a more important role in determining the SWV position. Thus, another four experiments are performed for each of the two sensitive regions by separating the vertical levels into the lower (below the 500 hPa level) and upper (above the 500 hPa level) half of the troposphere, i.e. A_PART_llq/ulq/llw/ulw for region A and B_PART_llq/ulq/llw/ulw for region B, where the footnotes 'llq/ulq/llw/ulw' refer to replacing the initial lower-level moisture (llq), upper-level moisture (ulq), the initial lower-level winds (llw) and upper-level winds (ulw) in the staggering m6 member with the corresponding field in the moving m5 member (see Table 1(c)). It is evident from Figure 14(a) that the SWV position is very sensitive to the initial lower-level moisture and upper-level wind perturbations but insensitive to the initial upper-level moisture and lower-level wind perturbations in the upstream region A. As a result, the SWV of the originally

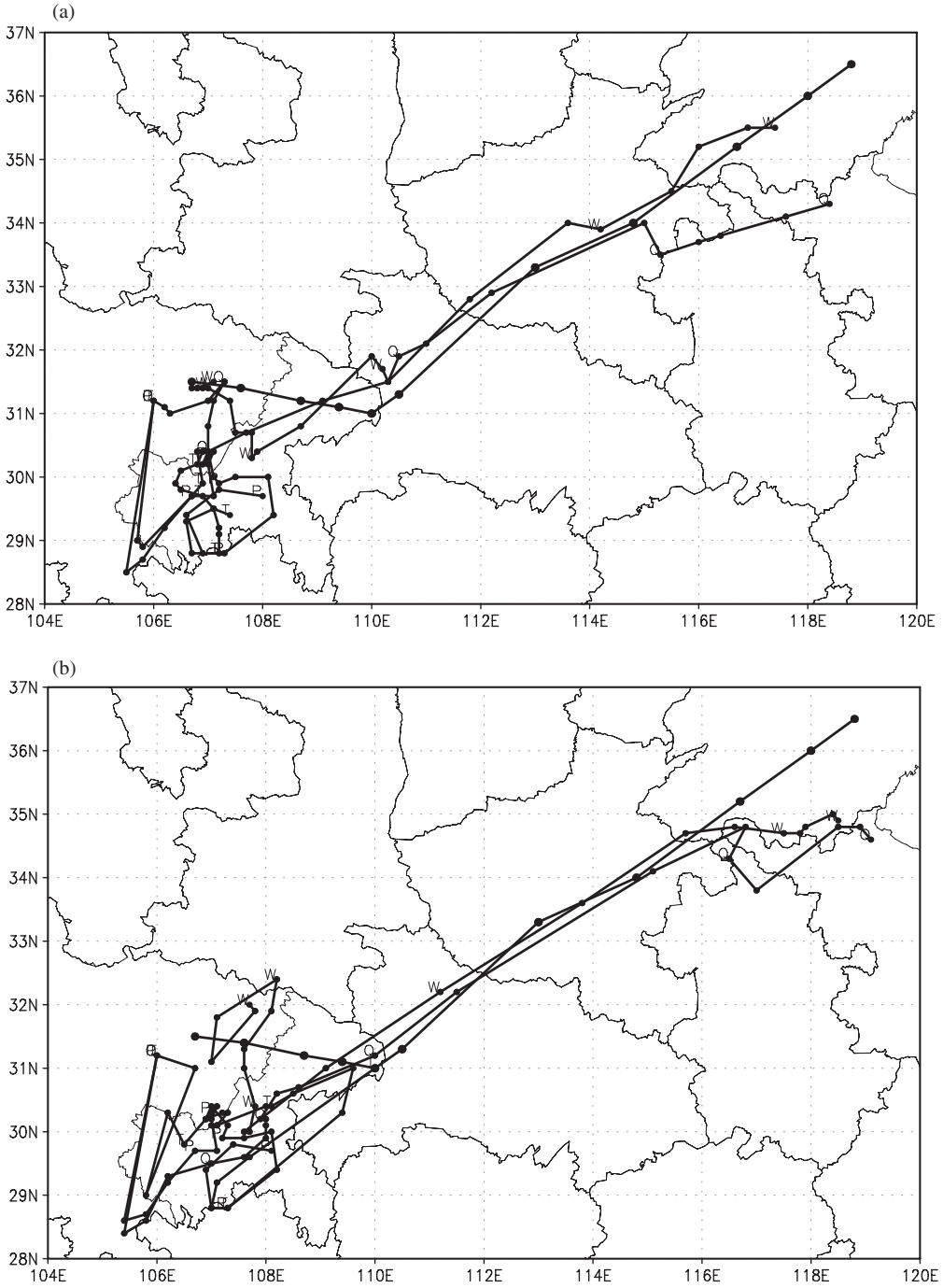

Figure 13. Same as Figure 10 but from the first group of the local-area sensitivity experiments over (a) region A and (b) region B.

staggering m6 member can successfully move out of the Sichuan Basin when either the initial lower-level moisture (A_PART_llq) or upper-level wind (A_PART_ulw) fields are replaced by the corresponding fields from the moving m5 member within box A. However, little change occurs when either the initial upper-level moisture (A_PART_ulq) or lower-level wind (A_PART_llw) field is replaced. This suggests that accurate ICs in the lower-level moisture and upper-level wind fields in the immediate upstream region of a vortex centre are important for obtaining an accurate forecast of SWVs. Figure 14(b) shows that for the downstream region B, the sensitivity of the SWV position forecast to the initial moisture perturbations is similar to that for the upstream region A, i.e. very sensitive to the initial lower-level moisture perturbations (B_PART_llq) but not to the initial upper-level moisture perturbations (B_PART_ulq). By contrast, its sensitivity to the initial wind perturbations is opposite to that of region A, i.e. more to the initial lower-level wind perturbations (B_PART_llw) than to the initial upper-level wind perturbations (B_PART_ulw). This result suggests that accurate ICs in both the lower-level moisture and wind in the immediate downstream region of the vortex centre are particularly important for obtaining an accurate SWV forecast.

Why does the sensitivity to initial moisture perturbations appear in the lower layers for both the downstream and upstream regions, whereas the sensitivity to initial wind perturbations occur in the lower layers for the downstream region but in the upper layers for the upstream region? We acknowledge that an in-depth study is needed to address fully the question raised above, but here we offer an explanation based on our own understanding. Before we address the above question, it should be borne in mind that a typical SWV is characterized by a closed circulation in the lower layers, with a trough aloft. This implies that any upper-level perturbations in the downstream region will be propagated away quickly and have less impact on the SWV, but the lower-level perturbations in either the upstream or downstream regions need to remain inside the vortex for a while to have an impact. As discussed previously, lower-level moist air in the downstream region favours a SWV to grow through latent

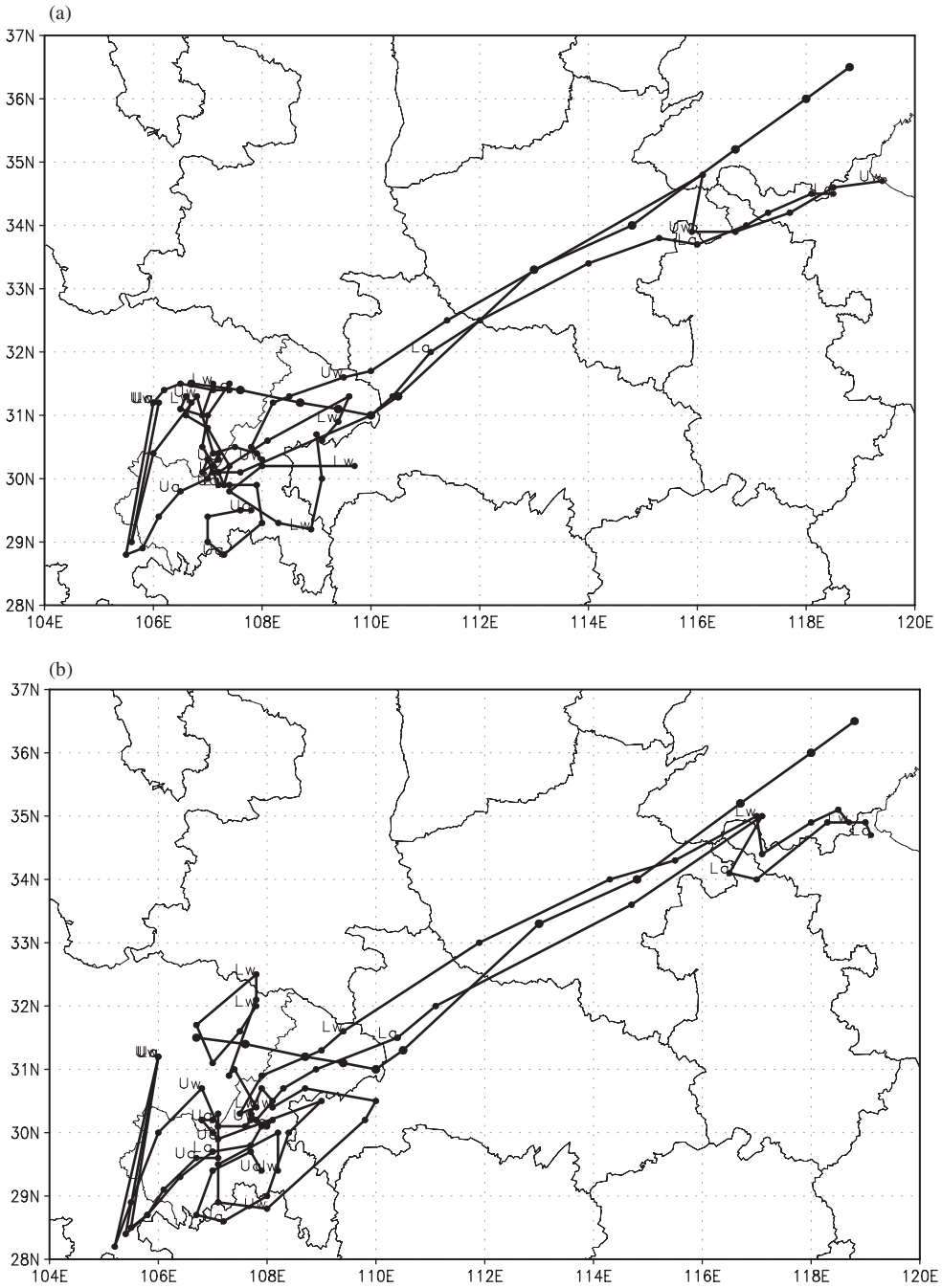

Figure 14. The predicted Southwest Vortex tracks from the second group of the local-area sensitivity experiments for (a) A_PART_llq/ulq/llw/ulw and (b) B_PART_llq/ulq/llw/ulw, together with the observed track (solid line with filled circles), where A_PART_llq and B_PART_llq are labelled 'Lq', A_PART_ulq and B_PART_ulq 'Uq', A_PART_llw and B_PART_llw 'Lw' and A_PART_ulw and B_PART_ulw 'Uw'.

heat release, whereas the dry air behind the SWV may produce strong moist downdrafts through dry intrusion, which would in turn favour the eastward movement of the SWV. By contrast, the lower-level wind perturbations in the downstream region are important because they mainly play a role in enhancing the lower-level moisture convergence for increased diabatic heating and for increased spin-up of the SWV, as indicated in Figure 9. The upper-level wind perturbations in the upstream region are important not only because they might affect the steering but, more importantly, also because they are in an area of dynamical instability, which may affect the SWV at a longer time-scale as all the wind perturbations move into the southwesterly flow ahead. To examine the changes in dynamical stability, further diagnosis using the potential vorticity and equivalent potential temperature fields is necessary. The low-level wind perturbations in the upstream region are not important because they are located in a region strongly affected by the unique topography near the eastern edge of the Tibetan Plateau, where the flow is dynamically and thermodynamically stable, although they could play a role in affecting the steering and the dry air intrusion process.

The above local-area sensitivity experiments demonstrate that modifying only a few selected IC variables within a small pre-chosen sensitive area could dramatically alter the outcome of a forecast – an effect equivalent to alternating ICs over the full model domain, although the response is a bit slower at the early stage. This result indicates the potential importance of using targeted observations in improving the short-range NWP of SWVs in terms of both intensity and displacement by focusing on a few key parameters in some key areas.

5. Summary and discussion

In this study, the track and growth of the 21 July 2008 SWV over southwest China are examined using a WRF-based REPS in order to demonstrate: (i) the usefulness of an EPS for understanding dynamical and thermodynamical conditions favourable for the

SWV's eastward movement and growth; and (b) the potential benefit of targeted-observation for improving short-range NWP using a simple technique. We acknowledge that any warm-season mesoscale weather system from any region around the world could be used to demonstrate the above two objectives, the reason why we chose an SWV case is because it is one of the important major weather systems in China and often brings extreme weather (heavy rain). In other words, the methodology demonstrated in this study should, in principle, be instructional and applicable to any other similar system around the world and not only to the SWV, although results may vary in detail.

Our results show significant variations in forecast performance, ranging from good to poor, among 11 ensemble members. By analysing two distinct groups ('moving' and 'staggering') of ensemble members, it is shown that the presence of a stronger upper-level trough aloft, a deeper pressure deficit associated with the lower-level convergence and positive vorticity ahead of the SWV centre, the westward vertical tilt, more (less) moisture content in the downstream enhanced southwesterly (upstream enhanced northwesterly) flow, and a more baroclinic environment facilitate the development of the SWV. It is found from the full-domain sensitivity experiments that SWV development is especially sensitive to the horizontal wind and moisture fields in the model initial conditions. The former appears to play an important role in the first 24 h of integrations, while the latter becomes more important with time as a result of the precipitation spin-up. These meteorologically insightful findings obtained from the 'ensemble analysis' approach demonstrate that ensemble forecast can provide a readily available basis for understanding the dynamical and thermodynamical characteristics of a weather system, e.g. the conditions leading to the development of SWVs in this study and probably other meteorological phenomena elsewhere.

An ensemble sensitivity experiment was then performed. A simplified correlation-based ensemble sensitivity approach was used to identify the regions in which the SWV position and intensity forecasts may be sensitive to the initial conditions. Two such sensitive regions are identified for this SWV case: one is located immediately upstream with prevailing northwesterly flow and the other immediately downstream with prevailing southwesterly flow, associated with the 500 hPa trough. With respect to the two sensitive areas, one group of the local-area sensitivity experiments was performed, which reveals significant (little) sensitivity of the SWV position forecasts to changes in the initial horizontal wind and moisture (temperature and SLP) conditions for both regions – a result similar to that seen in the full-domain sensitivity experiments but with a slower response especially in the early 12 h. Another group of local-area sensitivity experiments further shows that the SWV position forecast is sensitive to the initial horizontal winds in the upper (lower) half of the troposphere in the northwesterly upstream (southwesterly downstream) region, while it is sensitive to the initial moisture content in the lower half of the troposphere in both upstream and downstream regions. As a result, merely replacing one of these ICs – the lower-level moisture in either the upstream or downstream region, the upper-level horizontal wind in the upstream region or the lower-level horizontal wind in the downstream region – of a staggering member with the corresponding IC of a moving member would allow the originally quasi-stationary SWV to successfully move out of the Sichuan Basin. The fact that slightly modifying only a few selected IC variables within a small pre-chosen sensitive area could dramatically alter the outcome of a forecast demonstrates the great potential of applying a simple correlation based targeted observation technique for significantly improving short-range NWP. Through this approach, we could improve high-impact weather event forecasts by improving only the IC quality of a few pre-selected variables within pre-chosen key regions, case by case, rather than by improving all the ICs over a large coverage at all times. Based on this 'proof of concept' study, we suggest that field experiments of targeted observations can be designed potentially using this simple ensemble sensitivity approach to improve short-range NWP associated with SWVs. We are, however, aware that data assimilation procedures will adjust inserted observations for a balanced IC before the extra observation information can be used by an NWP model. Therefore, before conducting such a field experiment, an intermediate step should be taken to demonstrate that an 'improved' analysis resulted by adding a single (or a few) moisture sounding or wind profile data within an identified sensitive region can indeed produce desirable forecast outcome, similar to that shown by Zhang *et al.*. (2002, 2003).

It should be noted that consideration of the following three issues is required when applying our approach. First, the sensitivity of the SWV forecasts to the initial wind and moisture conditions suggests that obtaining accurate observations of the two fields and then properly assimilating them are critical to the improvement of short-range NWP of SWVs and probably to the other mesoscale convective systems, given the geostrophic adjustment constraint and the importance of diabatic heating. This appears to pose a challenging task in data assimilation because the two fields are unfortunately the most difficult ones to assimilate well (Kalnay, 2003). Second, the sensitive regions identified for targeted observations in short-range NWP are different from those in medium-range NWP. For the latter, sensitive areas, where extra observations may be needed, are normally related to a Rossby-wave envelope located in a distant upstream region (Hakim, 2003; Chang, 2005), whereas for the former, sensitive areas are not far upstream (unable to reach far within a short period), directly associated with the weather system of interest. This could provide a useful guidance for carrying out targeted observations for short-range NWP in general. Third, it should be mentioned that the results presented here are from one case study only. Clearly, more case studies are needed in order to generalize the above findings. In particular, a similar ensemble sensitivity study is needed for precipitation, because precipitation is an end product of a multiscale interaction among many complex processes, and it may not be as straightforward as the vortex position and intensity in terms of sensitive-region location. In addition, an in-depth analysis of the physical and dynamical processes associated with the IC perturbation evolution will also be helpful in designing better IC-perturbation generating schemes for mesoscale ensemble prediction systems.

In addition to the ES method applied herein, there are many other useful methods such as the adjoint and singular vector approaches (Palmer *et al.*, 1998; Pu *et al.*, 1998; Bergot, 1999; Bergot *et al.*, 1999; Buizza and Montani, 1999; Gelaro *et al.*, 1999; Langland *et al.*, 1999; Pu and Kalnay, 1999; Baker and Daley, 2000; Langland and Baker, 2004; Langland, 2005) and other ensemble-based approaches (Bishop and Toth, 1999; Szunyogh *et al.*, 2000, 2002; Morss *et al.*, 2001; Bishop *et al.*, 2001; Hamill and Synder, 2002) used for both targeted observation and sensitivity analysis (Hall *et al.*, 1982; Hall, 1986; Errico and Vukicevic, 1992; Rabier and Courtier, 1992; Errico *et al.*, 1993; Langland *et al.*, 1995; Rabier *et al.*, 1996; Zou *et al.*, 1998; Hoskins *et al.*, 2000; Langland *et al.*, 2002; Zhang *et al.*, 2002, 2003; Peng and Reynolds, 2006). Although a comparison of these methods is beyond the scope of this study, applications of other methods to SWVs will help us to determine how robust our results are. For example, some past studies indicate that a main difference between the adjoint and ES approaches is that the sensitivity revealed by the adjoint method is on a small-scale and confined within the lower troposphere with little connection to an actual weather system, whereas the sensitivity revealed by the ES method is on a synoptic scale that vertically penetrates throughout the entire troposphere with close connection to actual features of a weather system – although other studies may not fully agree with this assessment (e.g. see the discussions of Torn and Hakim (2008) and Ancell and Hakim (2007)). Therefore, it will be of interest to see which method is more suitable for SWVs.

Acknowledgements

This research was supported by NSFC41275107 and GYHY200906010. The first author (JL) would also like to thank the University of Maryland for hosting his 3-month visit at the Department of Atmospheric and Oceanic Science. DLZ was supported by NSF ATM0758609. We wish to thank Ms. Mary Hart, EMC/NCEP Information Officer, for her editorial assistance in improving the readability of this manuscript. The constructive comments and suggestions from Dr. Yong Wang and other two anonymous reviewers have greatly improved the quality of the article during the revision process.

References

Aberson SD. 2010. 10 years of hurricane synoptic surveillance (1997–2006). *Mon. Weath. Rev.* **138**: 1536–1549.

Ancell B, Hakim GJ. 2007. Comparing adjoint- and ensemble-sensitivity analysis with applications to observation targeting. *Mon. Weath. Rev.* **135**: 4117–4134.

Anderson JL. 2001. An ensemble adjustment Kalman filter for data assimilation. *Mon. Weath. Rev.* **129**: 2884–2903.

Baker NL, Daley R. 2000. Observation and background adjoint sensitivity in the adaptive observation targeting problem. *Q. J . R. Meteorol. Soc.* **126**: 1431–1454.

Bartels DL, Maddox RA. 1991. Midlevel cyclonic vortices generated by mesoscale convective systems. *Mon. Weath. Rev.* **119**: 104–118.

Bergot T. 1999. Adaptive observations during FASTEX: A systematic survey of upstream flights. *Q. J . R. Meteorol. Soc.* **125**: 3271–3298.

Bergot T, Hello G, Joly A, Malardel S. 1999. Adaptive observations: A feasibility study. *Mon. Weath. Rev.* **127**: 743–765.

Bishop CH, Toth Z. 1999. Ensemble transformation and adaptive observations. *J. Atmos. Sci.* **56**: 1748–1765.

Bishop CH, Etherton BJ, Majumdar SJ. 2001. Adaptive sampling with the ensemble transform Kalman filter. Part I: theoretical aspects. *Mon. Weath. Rev.* **129**: 420–436.

Blumen W. 1972. Geostrophic adjustment. *Rev. Geophys. Space Phys.* **10**: 485–528.

Buizza R, Montani A. 1999. Targeting observations using singular vectors. *J. Atmos. Sci.* **56**: 2965–2985.

Burpee RW, Franklin JL, Lord SJ, Tuleya RE, Aberson SD. 1996. The impact of Omega dropwindsondes on operational hurricane track forecast models. *Bull. Am. Meteorol. Soc.* **77**: 925–933.

Chang C-P, Yi, L, Chen GT-J. 2000. A numerical simulation of vortex development during the 1992 East Asian summer monsoon onset using the Navy's regional model. *Mon. Weath. Rev.* **128**: 1604–1631.

Chang EKM. 2005. The impact of wave packets propagating across Asia on Pacific cyclone development. *Mon. Weath. Rev.* **133**: 1998–2015.

Chen Z, Xu M, Min W. 2003. Relationship between abnormal activities of southwest vortex and heavy rain in the upper reach of Yangtze River during summer of 1998 (in Chinese). *Plateau Meteorol.* **22**: 162–167.

Chen Z, Min W, Miao Q, He G. 2004. A case study on coupling interaction between plateau and southwest vortexes (in Chinese). *Plateau Meteorol.* **23**: 75–80.

Chen T, Zhang F, Duan Y. 2011. A study of relationship between a southwest vortex and the mesoscale convective system during the severe '6.12' rainstorm event in Guangxi Province (in Chinese). *Acta Meteorol. Sin.* **69**: 472–485.

Davis C, Atkins N, Bartels D, Bosart L, Coniglio M, Bryan G, Cotton W, Dowell D, Jewett B, Johns R, Jorgensen D, Knievel J, Knupp K, Lee W-C, Mcfarquhar G, Moore J, Przybylinski R, Rauber R, Smull B, Trapp R, Trier S, Wakimoto R, Weisman M, Ziegler C. 2004. The Bow Echo and MCV Experiment: observations and opportunities. *Bull. Am. Meteorol. Soc.* **85**: 1075–1093.

Du J. 2007. Uncertainty and ensemble forecasting. *NOAA/NWS Science and Technology Infusion Lecture Series*, 42 pp. http://www.nws.noaa.gov/ost/climate/STIP/uncertainty.htm.

Du J, DiMego G, Toth Z, Jovic D, Zhou B, Zhu J, Chuang H, Wang J, Juang H, Rogers E, Lin Y. 2009. NCEP short-range ensemble forecast (SREF) system upgrade in 2009. *Nineteenth Conference on NWP and 23rd Conference on WAF*, American Meteorological Society. http://www.emc.ncep.noaa.gov/mmb/SREF/reference.html.

Emanuel K, Langland R. 1998. FASTEX adaptive observations workshop. *Bull. Am. Meteorol. Soc.* **79**: 1915–1919.

Errico RM, Vukicevic T. 1992. Sensitivity analysis using an adjoint of the PSU-NCAR mesoscale model. *Mon. Weath. Rev.* **120**: 1644–1660.

Errico RM, Vukicevic T, Raeder K. 1993. Comparison of initial and lateral boundary condition sensitivity for a limited -area model. *Tellus*, **45A**: 539–557.

Gelaro R, Langland RH, Rohaly GD, Rosmond TE. 1999. An assessment of the singular vector approach to targeted observations using the FASTEX data set. *Q. J. R. Meteorol. Soc.* **125**: 3299–3327.

Hakim GJ. 2003. Developing wave packets in the North Pacific storm track. *Mon. Weath. Rev.* **131**: 2824–2837.

Hakim GJ, Torn RD. 2008. Ensemble synoptic analysis. *Sanders Symp. Monogr. Meteorol. Monogr.* **33**: 147–162.

Hall MCG. 1986. Application of adjoint sensitivity theory to an atmospheric general circulation model. *J. Atmos. Sci.* **43**: 2644–2651.

Hall MCG, Cacuci DG, Schlesinger ME. 1982. Sensitivity analysis of a radiative convective model by the adjoint method. *J. Atmos. Sci.* **39**: 2083–2056.

Hamill TM, Snyder C. 2002. Using improved background error covariances from an ensemble Kalman filter for adaptive observations. *Mon. Weath. Rev.* **130**: 1552–1572.

Hamill TM, Snyder C, Morss RE. 2002. Analysis-error statistics of a quasi-geostrophic model using three-dimensional variational assimilation. *Mon. Weath. Rev.* **130**: 2777–2790.

Hoskins BJ, Buizza, R, Badger J. 2000. The nature of singular vector growth and structure. *Q. J. R. Meteorol. Soc.* **126**: 1565–1580.

Joly A, Jorgensen D, Shapiro MA, Thorpe A, Bessemoulin P, Browning KA, Cammas J-P, Chalon J-P, Clough SA, Emanuel KA, Eymard L, Gall R, Hildebrand PH, Langland RH, Lemaître Y, Lynch P, Moore JA, Persson PO, Snyder C, Wakimoto RM. 1997. The Fronts and Atlantic Storm-Track Experiment (FASTEX): Scientific objectives and experimental design. *Bull. Am. Meteorol. Soc.* **78**: 1917–1940.

Joly A, Keith A, Browning KA, Bessemoulin P, Cammas J-P, Caniaux G, Chalon J-P, Clough SA, Dirks R, Emanuel KA, Eymard L, Gall R, Hewson TD, Hildebrand PH, Jorgensen D, Lalaurette F, Langland RH, Lemaître Y, Mascart P, Moore JA, Persson PO, Roux F, Shapiro MA, Snyder C, Toth Z, Wakimoto RM. 1999. Overview of the field phase of the Fronts and Atlantic Storm-Track Experiment (FASTEX) project. *Q. J. R. Meteorol. Soc.* **125**: 3131–3163.

Kalnay E. 2003. *Atmospheric Modeling, Data Assimilation and Predictability*. Cambridge University Press: Cambridge; 341 pp.

Kuo Y-H, Cheng L, Bao J-W. 1988. Numerical simulation of the 1981 Sichuan flood. Part I: Evolution of a mesoscale southwest vortex. *Mon. Weath. Rev.* **116**: 2481–2504.

Langland RH. 2005. Issues in targeted observing. *Q. J. R. Meteorol. Soc.* **131**: 3409–3425.

Langland RH, Baker NL. 2004. Estimation of observation impact using the NRL atmospheric variational data assimilation adjoint system. *Tellus* **56A**: 189–201.

Langland RH, Elsberry RL, Errico RM. 1995. Evaluation of physical processes in an idealized extratropical cyclone using adjoint sensitivity. *Q. J. R. Meteorol. Soc.* **121**: 1349–1386.

Langland RH, Toth Z, Gelaro R, Szunyogh I, Shapiro MA, Majumdar SJ, Morss RE, Rohaly GD, Velden C, Bond N, Bishop CH. 1999. The North Pacific Experiment (NORPEX-98): Targeted observations for improved North American weather forecasts. *Bull. Am. Meteorol. Soc.* **80**: 1363–1384.

Langland RH, Shapiro MA, Gelaro R. 2002. Initial condition sensitivity and error growth in forecasts of the 25 January 2000 east coast snowstorm. *Mon. Weath. Rev.* **130**: 957–974.

Li J, Du J, Wang M, Cui C. 2009. The experiments of perturbing initial conditions in the development of mesoscale ensemble prediction system for heavy rain forecasting (in Chinese). *Plateau Meteorol.* **28**: 1365–1375.

Lu J. 1986. *Introduction to Southwest Vortex* (in Chinese). Meteorological Pres: Beijing; 270 pp.

Morss RE, Emanuel KA, Snyder C. 2001. Idealized adaptive observation strategies for improving numerical weather prediction. *J. Atmos. Sci.* **58**: 210–232.

Palmer TN, Gelaro R, Barkameijer J, Buizza R. 1998. Singular vectors, metrics, and adaptive observations. *J. Atmos. Sci.* **55**: 633–653.

Peng MS, Reynolds CA. 2006. Sensitivity of tropical cyclone forecasts as revealed by singular vectors. *J. Atmos. Sci.* **63**, 2508–2528.

Pu Z-X, Kalnay E. 1999. Targeting observation with the quasi-inverse linear and adjoint NCEP global models: performance during FASTEX. *Q. J. R. Meteorol. Soc.* **125**: 3329–3338.

Pu Z-X, Lord SJ, Kalnay E. 1998. Forecast sensitivity with dropwindsonde data and targeted observations. *Tellus* **50A**: 391–410.

Rabier F, Courtier P. 1992. Four-dimensional assimilation in the presence of baroclinic instability. *Q. J. R. Meteorol. Soc.* **118**: 649–672.

Rabier F, Klinker E, Courtier P, Hollingsworth A. 1996. Sensitivity of forecast errors to initial conditions. *Q. J. R. Meteorol. Soc.* **122**: 121–150.

Skamarock WC, Klemp JB, Dudhia J, Gill DO, Barker DM, Wang W, Powers JG. 2005. *A Description of the Advanced Research WRF, Version 2*. Technical Note 475+STR, National Centers for Atmospheric Research: Boulder, CO; 125 pp.

Snyder C. 1996. Summary of an informal workshop on adaptive observations and FASTEX. *Bull. Am. Meteorol. Soc*. **77**: 953–961.

Szunyogh I, Toth Z, Morss RC, Mujumdar SJ, Etherton BJ, Bishop CH. 2000. The effect of targeted dropsonde observations during the 1999 Winter Storm Reconnaissance Program. *Mon. Weath. Rev.* **128**: 3520–3537.

Szunyogh I, Toth Z, Zimin AV, Majumdar SJ, Persson A. 2002. Propagation of the effect of targeted observations: The 2000 Winter Storm Reconnaissance Program. *Mon. Weath. Rev.* **130**: 1144–1165.

Tao S-Y. 1980. *Heavy Rain in China* (in Chinese). Science Press: Beijing; 199 pp.

Torn RD, Hakim GJ. 2008. Ensemble-based sensitivity analysis. *Mon. Weath. Rev.* **136**: 663–677.

Toth Z, Kalnay E. 1993. Ensemble forecasting at NMC: The generation of perturbations. *Bull. Am. Meteorol. Soc.* **74**: 2317–2330.

Toth Z, Szunyogh I, Majumdar S, Morss R, Etherton B, Bishop C, Lord S, Ralph M, Persson O, Pu Z-X. 2000. Targeted observations at NCEP: Toward an operational implementation. *Preprints, 4th Symposium on Integrated Observation Systems*. American Meteorological Society: Boston, MA.

Tracton MS, Kalnay E. 1993. Operational ensemble prediction at the National Meteorological Center: Practical aspects. *Weath. Forecast.* **8**: 378–398.

Wang B. 1987. The development mechanism for Tibetan Plateau warm vortices. *J. Atmos. Sci.* **44**: 2978–2994.
Wang B, Orlanski I. 1987. Study of a heavy rain vortex formed over the eastern flank of the Tibetan Plateau. *Mon. Weath. Rev.* **115**: 1370–1393.
Wang W, Kuo Y-H, Warner TT. 1993. A diabatically driven mesoscale vortex in the lee of the Tibetan Plateau. *Mon. Weath. Rev.* **121**: 2542–2561.
Wang Z, Gao K. 2003. Sensitivity experiments of an eastward-moving southwest vortex to initial perturbations. *Adv. Atmos. Sci.* **20**: 638–649.
Wang Z-S, Wang Y, Liang Y. 1996. A numerical simulation study of a heavy rain event induced by a southwest vortex (in Chinese). In *Experimental, Synoptical and Dynamical Studies of Heavy Rain*. Meteorological Press: Beijing; 257–267.
Wei M, Toth Z, Wobus R, Zhu Y. 2008. Initial perturbations based on the ensemble transform (ET) technique in the NCEP global operational forecast system. *Tellus* **60A**: 62–79.
Wu G-X, Chen H. 1985. The effect of mechanical forcing on the formation of a mesoscale vortex. *Q. J. R. Meteorol. Soc.* **111**: 1049–1070.
Xu X, Chen L. 2006. Advances of the study on Tibetan Plateau experiment of atmospheric sciences (in Chinese). *J. Appl. Meteorol. Sci.* **17**: 756–772.
Zhang D-L, Fritsch JM. 1986. A case study of the sensitivity of numerical simulation of mesoscale convective systems to varying initial conditions. *Mon. Weath. Rev.* **114**: 2418–2431.
Zhang D-L, Fritsch JM. 1987. Numerical simulation of the meso-β-scale structure and evolution of the 1977 Johnstown flood. Part II: Inertially stable warm-core vortex and the mesoscale convective complex. *J. Atmos. Sci.* **44**: 2593–2612.
Zhang D-L, Fritsch JM. 1988. A numerical investigation of a convectively generated, inertially stable, extratropical warm-core mesovortex over land. Part I: Structure and evolution. *Mon. Weath. Rev.* **116**: 2660–2687.
Zhang F, Snyder C, Rotunno R. 2002. Mesoscale predictability of the 'surprise' snowstorm of 24–25 January 2000. *Mon. Weath. Rev.* **130**: 1617–1632.
Zhang F, Snyder C, Rotunno R. 2003. Effects of moist convection on mesoscale predictability. *J. Atmos. Sci.* **60**: 1173–1185.
Zhao Y, Wang Y. 2010. A case study on plateau vortex inducing southwest vortex and producing extremely heavy rain (in Chinese). *Plateau Meteorol.* **29**: 819–831.
Zou X, Kuo Y-H, Low-Nam S. 1998. Medium-range prediction of an extratropical oceanic cyclone: impact of initial state. *Mon. Weath. Rev.* **126**: 2737–2763.

